Abstracta

Ano XXII - N. 02

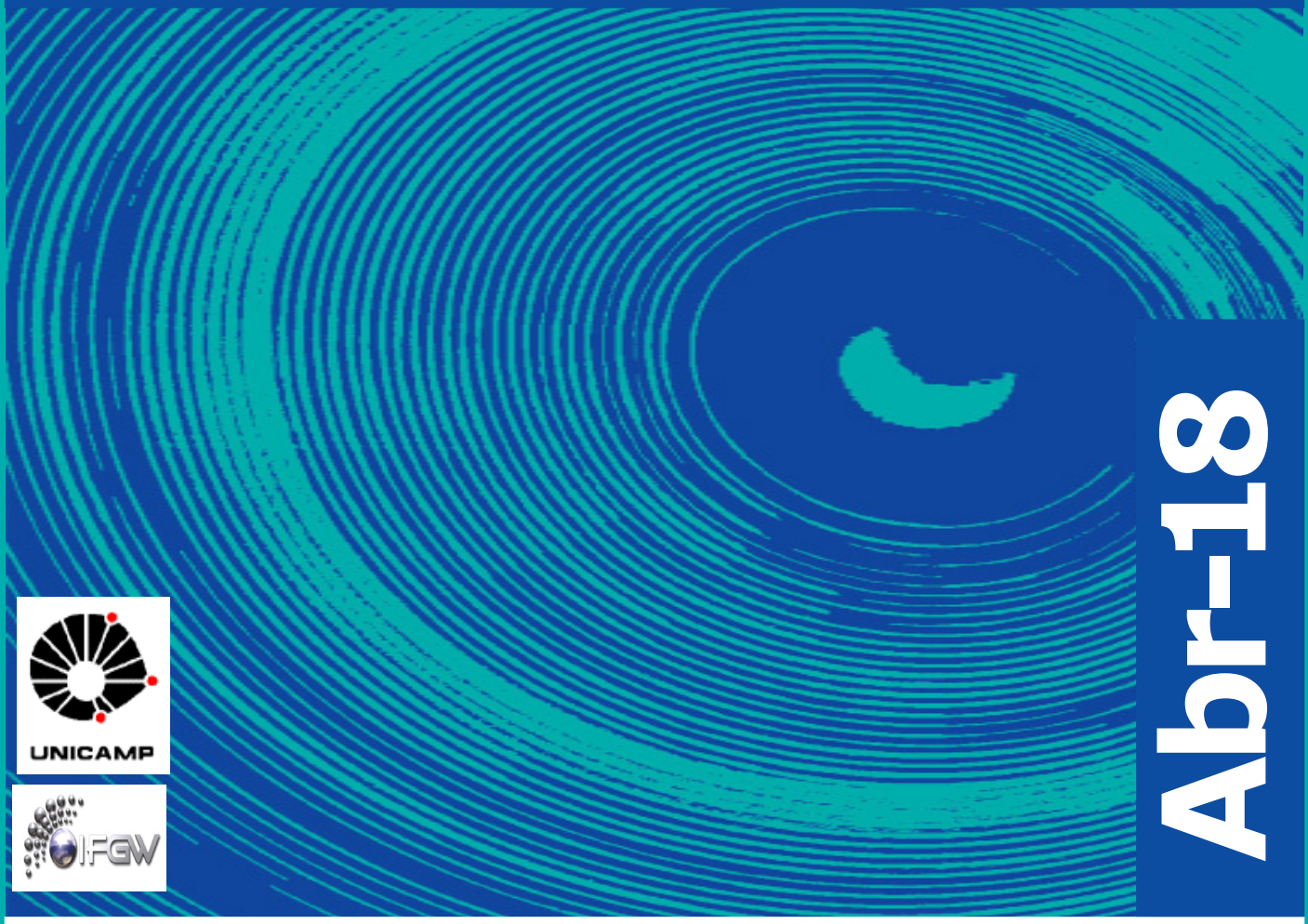

Abr-18

Artigos publicados - P021-2018 à P089-2018

Eventos publicados - P090-2018 à P091-2018

Correções - Co001-2018 à Co002-2018

Defesas de Dissertações do IFGW - D002-2018 à D007-2018

Defesas de Teses do IFGW - T006-2018 à T010-2018

Artigos publicados

[P021-2018] "A phenomenological approach to study the effect of uniaxial anisotropy on the magnetization of ferromagnetic nanoparticles"

Sanchez-Marin, N.; Cuchillo, A.; **Knobel, M.***; Vargas, P.

We study the effect of the uniaxial anisotropy in a system of ideal, noninteracting ferromagnetic nanoparticles by means of a thermodynamical model. We show that the effect of the anisotropy can be easily assimilated in a temperature shift T*(a), in analogy to what was proposed by Allia et al. (2001) in the case of interacting nanomagnets. The phenomenological anisotropic T*(a) parameter can be negative, indicating an antiferromagnetic-like behavior, or positive, indicating a ferromagnetic-like character as seen in the inverse susceptibility behavior as a function of temperature. The study is done considering an easy axis distribution to take into account the anisotropy axis dispersion in real samples (texture). In the case of a volumetric uniform distribution of anisotropy axes, the net effect makes T*(a) to vanish, and the magnetic susceptibility behaves like a conventional superparamagnetic system, whereas in the others a finite value is obtained for T*(a). When magnetic moment distribution is considered, the effect is to enhance the T*(a) parameter, when the dispersion of the magnetic moments becomes wider.

JOURNAL OF MAGNETISM AND MAGNETIC MATERIALS 452, 230-242, 2018. DOI: 10.1016/j.jmmm.2017.12.077

[P022-2018] "A theoretical and experimental investigation of Eu-doped ZnO nanorods and its application on dye sensitized solar cells"

Fonseca, A. F. V.; Siqueira, R. L.; **Landers, R***; Ferrari, J. L.; Marana, N. L.; Sambrano, J. R.; La Porta, F. D.; Schiavon, M. A.

This paper describes the electrodeposition of Europium-doped Zinc Oxide (ZnO) nanorods as well its application as photoanodes in dye sensitized solar cells (DSSCs). The incorporation of the Europium in the ZnO structure was evidenced by X-ray diffraction (XRD) and X-ray photoelectron spectroscopy (XPS). The DSSCs based on Eu-doped nanorods photoanodes exhibits a higher conversion efficiency value (h) (0.50%) compared to the undoped photoanodes (0.34%). Mott-Schottky analysis was performed and this increase is assigned to the better electronic injection efficiency from the dye to the conduction band of Eu-doped ZnO nanorods, since the Europium incorporation in the ZnO matrix was able to down-shift its conduction band. The improvement on the DSSC performance was around 45%, showing the great potential from the practical point of view. To complement the experimental data, computational simulations were employed based on DFT framework, in order to carry out a detailed analysis of the electronic structures of these materials, as well as to provide an elucidation of its underlying physical mechanism at an atomic level.

JOURNAL OF ALLOYS AND COMPOUNDS 739, 939-947, 2018. DOI: 10.1016/j.jallcom.2017.12.262

[P023-2018] "Adsorbate-Induced Modification of the Confining Barriers in a Quantum Box Array"

Nowakowska, S.; Mazzola, F.; Alberti, M. N.; Song, F.; Voigt, T.; Nowakowski, J.; Wackerlin, A.; Wackerlin, C.; Wiss, J.; Schweizer, W. B.; Broszio, M.; Polley, C.; Leandersson, M.; **Fatayer, S.***; Ivas, T.; Baljozovic, M.; Mousavi, S. F.; Ahsan, A.; Nijs, T.; Popova, O.; Zhang, J.; Muntwiler, M.; Thilgen, C.; Stohr, M.; Pasti, I. A.; Skorodumova, N. V.; Diederich, F.; Wells, J.; Jung, T. A.

Quantum devices depend on addressable elements, which can be modified separately and in their mutual interaction. Self-assembly at surfaces, for example, formation of a porous (metal-) organic network, provides an ideal way to manufacture arrays of identical quantum boxes, arising in this case from the confinement of the electronic (Shockley) surface state within the pores. We show that the electronic quantum box state as well as the interbox coupling can be modified locally to a varying extent by a selective choice of adsorbates, here C-60, interacting with the barrier. In view of the wealth of differently acting adsorbates, this approach allows for engineering quantum states in on-surface network architectures.

ACS NANO 12(1), 768-778, 2018. DOI: 10.1021/acsnano.7b07989

[P024-2018] "An Indication of Anisotropy in Arrival Directions of Ultra-high-energy Cosmic Rays through Comparison to the Flux Pattern of Extragalactic Gamma-Ray Sources"

Aab, A.; Abreu, P.; Aglietta, M.; **Chinellato, J. A.*; Daniel, B.*; Diaz Castro, M. L.*; Dobrigkeit, C.*; Fauth, A. C.*; Kemp, E.*; Muller, M. A.*; Pereira, L. A. S.*; Theodoro, V. M.***; et al. Pierre Auger Collaboration

A new analysis of the data set from the Pierre Auger Observatory provides evidence for anisotropy in the arrival directions of ultra-high-energy cosmic rays on an intermediate angular scale, which is indicative of excess arrivals from strong, nearby sources. The data consist of 5514 events above 20 EeV with zenith angles up to 80 degrees. recorded before 2017 April 30. Sky models have been created for two distinct populations of extragalactic gamma-ray emitters: active galactic nuclei from the second catalog of hard Fermi-LAT sources (2FHL) and starburst galaxies from a sample that was examined with Fermi-LAT. Flux-limited samples, which include all types of galaxies from the Swift-BAT and 2MASS surveys, have been investigated for comparison. The sky model of cosmic-ray density constructed using each catalog has two free parameters, the fraction of events correlating with astrophysical objects, and an angular scale characterizing the clustering of cosmic rays around extragalactic sources. A maximum-likelihood ratio test is used to evaluate the best values of these parameters and to quantify the strength of each model by contrast with isotropy. It is found that the starburst model fits the data better than the hypothesis of isotropy with a statistical significance of 4.0 sigma, the highest value of the test statistic being for energies above 39 EeV. The three alternative models are favored against isotropy with 2.7 sigma-3.2 sigma significance. The origin of the indicated deviation from isotropy is examined and prospects for more sensitive future studies are discussed.

ASTROPHYSICAL JOURNAL LETTERS 853(2), L29, 2018. DOI: 10.3847/2041-8213/aaa66d

[P025-2018] "Anisotropic growth of alpha-Fe2O3 nanostructures"

Jesus, J. R.; Lima, R. J. S.; **Moura, K. O.***; Duque, J. G. S.; Meneses, C. T.

In this work, we report on the anisotropic growth of alpha-Fe2O3 nanoslabs which are produced by co-precipitation method with the addition of sucrose. In our previous work, we have argued that such behavior can be related with the chelating agent. Experiments of X-ray diffraction (XRD), high-resolution transmission electronic microscopy (HRTEM) and magnetic measurements as a function of temperature and an applied magnetic field are used to characterize the samples. The HRTEM image of the sample prepared with 10 mmol/l of sucrose consists of faceted-like nanoslabs while that prepared without sucrose exhibits particles with a non-uniform shape.

In this way, we can state that both the HRTEM images and the analysis of the XRD patterns show clearly a preferential growth of the [110] crystallographic direction. To strengthen our supposition, besides T- and field-dependence of magnetization are consistent with a superparamagnetic behavior the fit of the (Zero Field Cooling and Field Cooling) ZFC-FC curve for sample grown with 10 mmol/l of sucrose presents a strong increase of the effective anisotropy constant, K-eff, which can be related with the increasing of the shape magnetic anisotropy.

CERAMICS INTERNATIONAL 44(4), 3585-3589, 2018. DOI: 10.1016/j.ceramint.2017.11.068

[P026-2018] "Automated quantum operations in photonic qutrits"

Borges, G. F.; **Baldijao, R. D.***; Conde, J. G. L.; Cabral, J. S.; Marques, B.; Terra Cunha, M.; Cabello, A.; Padua, S.

We report an experimental implementation of automated state transformations on spatial photonic qutrits following the theoretical proposal made by Baldijao et al. [Phys. Rev. A 96, 032329 (2017)]. A qutrit state is simulated by using three Gaussian beams, and after some state operations, the transformed state is available in the end in terms of the basis state. The state transformation setup uses a spatial light modulator and a calcite-based interferometer. The results reveal the usefulness of the operation method. The experimental data show a good agreement with theoretical predictions, opening possibilities for explorations in higher dimensions and in a wide range of applications. This is a necessary step in qualifying spatial photonic qudits as a competitive setup for experimental research in the implementation of quantum algorithms which demand a large number of steps.

PHYSICAL REVIEW A 97(2), 022301, 2018. DOI: 10.1103/PhysRevA.97.022301

[P027-2018] "Azimuthal anisotropy of charged particles with transverse momentum up to 100GeV/c in PbPb collisions at root S-NN=5.02 TeV"

Sirunyan, A. M.; Tumasyan, A.; Adam, W.; **Chinellato, J. A.*; Tonelli Manganote, E. J.***; et al.
CMS Collaboration

The Fourier coefficients v(2) and v(3) characterizing the anisotropy of the azimuthal distribution of charged particles produced in PbPb collisions at root S-NN = 5.02 TeV are measured with data collected by the CMS experiment. The measurements cover a broad transverse momentum range, 1 < p(T) < 100 GeV/c. The analysis focuses on the p(T) > 10 GeV/c range, where anisotropic azimuthal distributions should reflect the path-length dependence of parton energy loss in the created medium. Results are presented in several bins of PbPb collision centrality, spanning the 60% most central events. The v(2) coefficient is measured with the scalar product and the multiparticle cumulant methods, which have different sensitivities to initial-state fluctuations. The values from both methods remain positive up to p(T) similar to 60-80 GeV/c, in all examined centrality classes. The v(3) coefficient, only measured with the scalar product method, tends to zero for p(T) greater than or similar to 20 GeV/c. Comparisons between theoretical calculations and data provide new constraints on the path-length dependence of parton energy loss in heavy ion collisions and highlight the importance of the initial-state fluctuations.

PHYSICS LETTERS B 776, 195-216, 2018. DOI: 10.1016/j.physletb.2017.11.041

[P028-2018] "Brightness and uniformity measurements of plastic scintillator tiles at the CERN H2 test beam"

Chatrchyan, S.; Sirunyan, A. M.; Tumasyan, A.; **Chinellato, J. A.*; Tonelli Manganote, E. J.***; et al.
CMS HCAL Collaboration

We study the light output, light collection efficiency and signal timing of a variety of organic scintillators that are being considered for the upgrade of the hadronic calorimeter of the CMS detector. The experimental data are collected at the H2 test-beam area at CERN, using a 150 GeV muon beam. In particular, we investigate the usage of over--doped and green-emitting plastic scintillators, two solutions that have not been extensively considered. We present a study of the energy distribution in plastic-scintillator tiles, the hit efficiency as a function of the hit position, and a study of the signal timing for blue and green scintillators.

JOURNAL OF INSTRUMENTATION 13, P01002, 2018. DOI: 10.1088/1748-0221/13/01/P01002

[P029-2018] "Center-of-Mass Acceleration in Coupled Nanowaveguides Due to Transverse Optical Beating Force"

Fernandes, T. F. D.; **Carvalho, C. M. K. C.***; Guimaraes, P. S. S.; Neves, B. R. A.; **de Assis, P. L.***

Eigenmode optical forces arising in symmetrically coupled waveguides have opposite sign on opposite waveguides and thus can deform the waveguides by changing their relative separation, but cannot change any other degree of freedom on their own. It would be extremely desirable to have a way to act on the center of mass of such a system. In this work, we show that it is possible to do so by injecting a superposition of eigenmodes that are degenerate in frequency and have opposite parity along the desired direction, resulting in beating forces that have the same sign on opposite waveguides and, therefore, act on the center of mass. We have used both the Maxwell stress tensor formalism and the induced dipole force equation to numerically calculate this transverse beating force and have found itsmagnitude to be comparable to the eigenmode forces. We also show that the longitudinal variation caused by the spatial beating pattern on the time-averaged quantities used in the calculations must be taken into account in order to properly employ the divergence theorem and obtain the correct magnitudes. We then propose a heuristic model that shows good quantitative agreement with the numerical results and may be used as a prototyping tool for accurate and fast computation without relying on expensive numerical computation.

JOURNAL OF LIGHTWAVE TECHNOLOGY 36(9), 1608-1614, 2018. DOI: 10.1109/JLT.2017.2784856

[P030-2018] "Comparative study of post-growth annealing of Cu(hfac)(2), Co-2(CO)(8) and Me2Au(acac) metal precursors deposited by FEBID"

dos Santos, M. V. P.*; Szkudlarek, A.; Rydosz, A.; Guerra-Nunez, C.; **Beron, F.*; Pirota, K. R.***; Moshkalev, S.; Diniz, J. A.; Utke, I.

Non-noble metals, such as Cu and Co, as well as noble metals, such as Au, can be used in a number modern technological applications, which include advanced scanning-probe systems, magnetic memory and storage, ferroelectric tunnel junction memristors, metal interconnects for high performance integrated circuits in microelectronics and nano-optics applications, especially in the areas of plasmonics and metamaterials. Focused-electron-beam-induced deposition (FEBID) is a maskless direct-write tool capable of defining 3-dimensional metal deposits at nanometre scale for above applications.

However, codeposition of organic ligands when using organometallic precursors is a typical problem that limits FEBID of pure metal nanostructures. In this work, we present a comparative study using a post-growth annealing protocol at 100, 200, and 300 degrees C under high vacuum on deposits obtained from Co-2(CO)(8), Cu(II)(hfac)(2), and Me2Au(acac) to study improvements on composition and electrical conductivity. Although the as-deposited material was similar for all precursors, metal grains embedded in a carbonaceous matrix, the post-growth annealing results differed. Cu-containing deposits showed the formation of pure Cu nanocrystals at the outer surface of the initial deposit for temperatures above 100 degrees C, due to the migration of Cu atoms from the carbonaceous matrix containing carbon, oxygen, and fluorine atoms. The average size of the Cu crystals doubles between 100 and 300 degrees C of annealing temperature, while the composition remains constant. In contrast, for Co-containing deposits oxygen release was observed upon annealing, while the carbon content remained approximately constant; the cobalt atoms coalesced to form a metallic film. The as-deposited Au-containing material shows subnanometric grains that coalesce at 100 degrees C, maintaining the same average size at annealing temperatures up to 300 degrees C. Raman analysis suggests that the amorphous carbonaceous matrix of the as-written Co, Cu and Au deposits turned into nanocrystalline graphite with comparable crystal sizes of 12-14 nm at 300 degrees C annealing temperature. However, we observed a more effective formation of graphite clusters in Co- than in Cu- and Au-containing deposits. The graphitisation has a minor influence on the electrical conductivity improvements of Co-C deposits, which is attributed to the high as-deposited Co content and the related metal grain percolation. On the contrary, electrical conductivity improvements by factors of 30 and 12 for, respectively, Cu-C and Au-C deposits with low metal content are mainly attributed to the graphitisation. This relatively simple vacuum-based post--growth annealing protocol may be useful for other precursors as it proved to be efficient in reliably tuning the electrical properties of as-deposited FEBID materials. Finally, a H-2-assisted gold purification protocol is demonstrated at temperatures around 300 degrees C by fully removing the carbon matrix and drastically reducing the electrical resistance of the deposit.

BEILSTEIN JOURNAL OF NANOTECHNOLOGY 9, 91-101, 2018. DOI: 10.3762/bjnano.9.11

[P031-2018] "Constraining the magnitude of the Chiral Magnetic Effect with Event Shape Engineering in Pb-Pb collisions at root s(NN)=2.76 TeV"

Acharya, S.; Adam, J.; Adamova, D.; **Albuquerque, D. S. D.*; Chinellato, D. D.*; De Souza, R. D.*; Takahashi, J.***; et al.
ALICE Collaboration

In ultrarelativistic heavy-ion collisions, the event-by-event variation of the elliptic flow v(2) reflects fluctuations in the shape of the initial state of the system. This allows to select events with the same centrality but different initial geometry. This selection technique, Event Shape Engineering, has been used in the analysis of charge-dependent two-and three-particle correlations in Pb-Pb collisions at root s(NN) = 2.76 TeV. The two--particle correlator < cos(phi(alpha) - phi(ss))>, calculated for different combinations of charges alpha and beta, is almost independent of v(2) (for a given centrality), while the three-particle correlator < cos(phi(alpha) + phi(beta) - 2 Psi(2))> scales almost linearly both with the event v(2) and charged-particle pseudorapidity density. The charge dependence of the three--particle correlator is often interpreted as evidence for the Chiral Magnetic Effect (CME), a parity violating effect of the strong interaction. However, its measured dependence on v(2) points to a large non-CME contribution to the correlator. Comparing the results with Monte Carlo calculations including a magnetic field due to the spectators, the upper limit of the CME signal contribution to the three-particle correlator in the 10-50% centrality interval is found to be 26-33% at 95% confidence level.

PHYSICS LETTERS B 777, 151-162, 2018. DOI: 10.1016/j.physletb.2017.12.021

[P032-2018] "Constraintson the double-parton scattering cross section from same-sign W boson pair production in proton-proton collisions at root s=8TeV"

Sirunyan, A. M.; Tumasyan, A.; Adam, W.; **Chinellato, J. A.*; Tonelli Manganote, E. J.***; et al.
CMS Collaboration

A first search for same-sign WW production via double-parton scattering is performed based on proton-proton collision data at a center-of-mass energy of 8TeV using dimuon and electron-muon final states. The search is based on the analysis of data corresponding to an integrated luminosity of 19.7 fb(-1). No significant excess of events is observed above the expected single-parton scattering yields. A 95% confidence level upper limit of 0.32 pb is set on the inclusive cross section for same-sign WW production via the double-parton scattering process. This upper limit is used to place a 95% confidence level lower limit of 12.2mb on the effective double--parton cross section parameter, closely related to the transverse distribution of partons in the proton. This limit on the effective cross section is consistent with previous measurements as well as with Monte Carlo event generator predictions.

JOURNAL OF HIGH ENERGY PHYSICS 2, 032, 2018. DOI: 10.1007/JHEP02(2018)032

[P033-2018] "Crystallization of low saturated lipid blends of palm and canola oils with sorbitan monostearate and fully hydrogenated palm oil"

Barbosa, K. M.; **Cardoso, L. P.***; Ribeiro, A. P. B.; Kieckbusch, T. G.; Buscato, M. H. M.

Several scientific investigations have focused on providing new strategies for supporting the development of low saturated and zero trans lipid materials, as healthier fat alternatives for food application. This work evaluated the consistency, crystallization behavior, microstructure and polymorphism of six blends composed of palm and canola oils at different concentrations (100:0, 80:20, 60:40, 40:60, 20:80 and 0:100, in w/w%) added with 5.0% of fully hydrogenated palm oil (FHPO) or with a mixture of 2.5% of FHPO and 2.5% of sorbitan monostearate (SMS). The results were compared with the non-structured blends (standard samples). Through microstructure images, the formation of a more homogeneous and denser packed crystal network was observed for samples added with both crystallization modifiers (FHPO/SMS) compared to the corresponding standard samples, after stabilization at 25 A degrees C during 3 h. In particular, enhanced crystallization modifications were observed for the 40:60 blend, in which the crystal form beta' emerged after the addition of FHPO/SMS. Moreover, the 40:60 blend structured with FHPO/SMS showed increased consistency (from 30 to 658 g(F)/cm(2)) and induced onset crystallization in a higher temperature (from 13.1 to 23.9 A degrees C) compared with the non-structured one, due to the specific crystallization effects provided by both added structurants.

JOURNAL OF FOOD SCIENCE AND TECHNOLOGY-MYSORE 55(3), 1104-1115, DOI: 10.1007/s13197-017-3026-5

[P034-2018] "D-Meson Azimuthal Anisotropy in Midcentral Pb-Pb Collisions root S-NN=5.02 TeV"

Acharya, S.; Adamova, D.; Adolfsson, J.; **Albuquerque, D. S. D.*; Chinellato, D. D.*; De Souza, R. D.*; Takahashi, J.***;
ALICE Collaboration

The azimuthal anisotropy coefficient v(2) of prompt D-0, D+, D*+, and D-s(+) mesons was measured in midcentral (30%-50% centrality class) Pb-Pb collisions at a center-of-mass energy per nucleon pair root s(NN)=5.02 TeV, with the ALICE detector at the LHC. The D mesons were reconstructed via their hadronic decays at midrapidity, |y| < 0.8, in the transverse momentum interval 1 < p(T) < 24 GeV/c. The measured D--meson v(2) has similar values as that of charged pions. The D-s(+) v(2), measured for the first time, is found to be compatible with that of nonstrange D mesons. The measurements are compared with theoretical calculations of charm--quark transport in a hydrodynamically expanding medium and have the potential to constrain medium parameters.

PHYSICAL REVIEW LETTERS 120(10), 102301, 2018. DOI: 10.1103/PhysRevLett.120.102301

[P035-2018] "Damping of Landau levels in neutral graphene at low magnetic fields: A phonon Raman scattering study"

Ardito, F. M.*; Mendes-de-Sa, T. G.; Cadore, A. R.; **Gomes, P. F.***; Mafra, D. L.; Barcelos, I. D.; Lacerda, R. G.; **Iikawa, F.*; Granado, E.***

Landau level broadening mechanisms in electrically neutral and quasineutral graphene were investigated through micro--magneto-Raman experiments in three different samples, namely, a natural single-layer graphene flake and a back-gated single-layer device, both deposited over Si/SiO2 substrates, and a multilayer epitaxial graphene employed as a reference sample. Interband Landau level transition widths were estimated through a quantitative analysis of the magnetophonon resonances associated with optically active Landau level transitions crossing the energy of the E-2g Raman-active phonon. Contrary to multilayer graphene, the single-layer graphene samples show a strong damping of the low-field resonances, consistent with an additional broadening contribution of the Landau level energies arising from a random strain field. This extra contribution is properly quantified in terms of a pseudomagnetic field distribution Delta B = 1.0 - 1.7 T in our single-layer samples.

PHYSICAL REVIEW B 97(3), 035419, 2018. DOI: 10.1103/PhysRevB.97.035419

[P036-2018] "Design of a compact CMOS-compatible photonic antenna by topological optimization"

Pita, J. L.; **Aldaya, I.*; Dainese, P.***; Hernandez-Figueroa, H. E.; Gabrielli, L. H.

Photonic antennas are critical in applications such as spectroscopy, photovoltaics, optical communications, holography, and sensors. In most of those applications, metallic antennas have been employed due to their reduced sizes. Nevertheless, compact metallic antennas suffer from high dissipative loss, wavelength-dependent radiation pattern, and they are difficult to integrate with CMOS technology. All-dielectric antennas have been proposed to overcome those disadvantages because, in contrast to metallic ones, they are CMOS-compatible, easier to integrate with typical silicon waveguides, and they generally present a broader wavelength range of operation. These advantages are achieved, however, at the expense of larger footprints that prevent dense integration and their use in massive phased arrays. In order to overcome this drawback, we employ topological optimization to design an all-dielectric compact antenna with vertical emission over a broad wavelength range. The fabricated device has a footprint of 1.78 mu m x 1.78 mu m and shows a shift in the direction of its main radiation lobe of only 4 degrees over wavelengths ranging from 1470 nm to 1550 nm and a coupling efficiency bandwidth broader than 150 nm.

OPTICS EXPRESS 26(3), 2435-2442, 2018. DOI: 10.1364/OE.26.002435

[P037-2018] "Electrothermal silver nanowire thin films for In-Situ observation of thermally-driven chemical processes"

Martinez, E. D.*; Flores, A. F. G.; Pastoriza, H.; **Urbano, R. R.*; Rettori, C.***

We develop a novel device comprised of high optical transmittance thin films containing silver nanowires (AgNWs) in poly(methyl methacrylate) (PMMA) acting as heating elements. The electrothermal control of the AgNWs network allows us to externally trigger and tune the temperature conditions required to run chemical reactions and physicochemical processes. The device was successfully applied for the spectroscopic in-situ observation of three different model reactions: i) the thermal equilibrium of a CoCl2/HCl/H2O complex, ii) the reversible macromolecular phase transition of a pNIPAM solution, and iii) the nucleation and growth of gold nanoparticles (AuNPs). In the first case, the color of the CO2+ complex was reversibly switched from pink to blue when changing the thermal equilibrium condition. In the second one, the optical transmittance of an aqueous solution of carboxylic-terminated pNIPAM polymer was cycled from high to low as the temperature of the solution was below or above the lower critical solubility temperature (LCST) respectively. Finally, the electrothermal control on the device was applied to the study of the nucleation and growth of AuNPs in an organic solution of AuCl3 containing oleylamine acting as both the reducer and the stabilizing agent. The versatility of the electrothermal device provides an easy way to undertake thermally controlled processes and develop optical elements such as smart windows and lab-on-a-chip devices. The AgNWs-PMMA nanocomposite was also applied successfully as an electrothermal ink on the external side walls of a test tube.

SENSORS AND ACTUATORS B-CHEMICAL 259, 475-483, 2018. DOI: 10.1016/j.snb.2017.12.021

[P038-2018] "Exotic magnetism and spin-orbit-assisted Mott insulating state in a 3d-5d double perovskite"

Cavichini, A. S.; Orlando, M. T.; Depianti, J. B.; Passamai, J. L.; Damay, F.; Porcher, F.; **Granado, E.***

Themagnetic structure of Ca2MnReO6 double perovskite is investigated by neutron powder diffraction and bulk magnetization, showing dominant noncollinear Mn magnetic moments [4.35(7) mu(B)] that are orthogonally aligned with the small Re moments [0.22(4) mu(B)]. Ab initio electronic structure calculations show that the strong spin-orbit coupling for Re 5d electrons combined with a relatively modest on-site Coulomb repulsion (U-eff(Re) greater than or similar to 0.6 eV) is sufficient to render this material insulating. This is a rare example of spin-orbit-assisted Mott insulator outside the realm of iridates, with remarkable magnetic properties.

PHYSICAL REVIEW B 97(5), 054431, 2018. DOI: 10.1103/PhysRevB.97.054431

[P039-2018] "Experimental realisation of off-stoichiometric Fe-Mn-Si full Heusler alloy with hexagonal crystal structure by pulsed laser deposition"

Checca, N. R.; Caraballo-Vivas, R. J.; **Coelho, A. A.***; Rossi, A.; Fortunato, N. M.; Mohseni, F.; Goncalves, J. N.; Amaral, J. S.; Rocco, D. L.; Reis, M. S.

Full Heusler alloys are well known to either crystallize in a cubic structure (Cu2MnAl-type), or present tetragonal distortions. Both structure types present interesting properties, like room temperature magnetic memory shape effect and/or remarkable magnetocaloric effect, mainly ruled by strong magnetostructural coupling.

Due to this interplay, our aim was to produce a new crystal phase for the Heusler alloys, different from those well-established cubic and tetragonal, responsible for those well-known physical properties. Thus, we have produced nanoparticles of full Heusler alloys using a pulsed laser deposition technique (from targets of Fe2MnSi) and obtained a core-shell pattern, presenting an amorphous shell and a crystalline core, with hexagonal symmetry. In accordance with these experimental findings, it was shown, by means of density functional calculation, the existence of a minimum of energy as a function of the hexagonal lattice parameters, with a true indication that the hexagonal phase is metastable. The magnetic properties differ considerably from those of bulk Fe2MnSi, including an increase of the Curie temperature from 220 K to 295 K, which is of potential interest for room-temperature applications. This work opens the door to research in a new family of materials, whose properties have only now begun to be explored.

MATERIALS & DESIGN 143, 268-273, 2018. DOI: 10.1016/j.matdes.2018.01.062

[P040-2018] "Extreme Variability Quasars from the Sloan Digital Sky Survey and the Dark Energy Survey"

Rumbaugh, N.; Shen, Y.; Morganson, E.; **Sobreira, F.***; et al. DES Collaboration

We perform a systematic search for long-term extreme variability quasars (EVQs) in the overlapping Sloan Digital Sky Survey and 3 Year Dark Energy Survey imaging, which provide light curves spanning more than 15 years. We identified similar to 1000 EVQs with a maximum change in g-band magnitude of more than 1 mag over this period, about 10% of all quasars searched. The EVQs have L-bol similar to 10(45)-10(47) erg s(-1) and L/L--Edd similar to 0.01-1. Accounting for selection effects, we estimate an intrinsic EVQ fraction of similar to 30%-50% among all g less than or similar to 22 quasars over a baseline of similar to 15 yr. We performed detailed multi-wavelength, spectral, and variability analyses for the EVQs and compared them to their parent quasar sample. We found that EVQs are distinct from a control sample of quasars matched in redshift and optical luminosity: (1) their UV broad emission lines have larger equivalent widths; (2) their Eddington ratios are systematically lower; and (3) they are more variable on all timescales. The intrinsic difference in quasar properties for EVQs suggests that internal processes associated with accretion are the main driver for the observed extreme long-term variability. However, despite their different properties, EVQs seem to be in the tail of a continuous distribution of quasar properties, rather than standing out as a distinct population. We speculate that EVQs are normal quasars accreting at relatively low rates, where the accretion flow is more likely to experience instabilities that drive the changes in flux by a factor of a few on multi-year timescales.

ASTROPHYSICAL JOURNAL 854(2) 160, 2018. DOI: 10.3847/1538-4357/aaa9b6

[P041-2018] "Femtosecond laser micromachining of polylactic acid/graphene composites for designing interdigitated microelectrodes for sensor applications"

Paula, K. T.; Gaal, G.; Almeida, G. F. B.; Andrade, M. B.; Facure, M. H. M.; Correa, D. S.; **Riul, A.*; Rodrigues, V.***; Mendonca, C. R.

There is an increasing interest in the last years towards electronic applications of graphene-based materials and devices Fabricated from patterning techniques. with the ultimate goal of high performance and temporal resolution. Laser micromachining using femtosecond pulses is an attractive methodology to integrate graphene-based materials into functional devices as it allows changes to the focal volume with a submicrometer spatial resolution due to the efficient nonlinear nature of the absorption, yielding rapid prototyping for innovative applications. We present here the patterning of PLA-graphene films spin coated on a glass substrate using a fs-laser at moderate pulse energies to fabricate interdigitated electrodes having a minimum spatial resolution of 5 pm. Raman spectroscopy of the PLA-graphene films indicated the presence of multilayered graphene fibers. Subsequently, the PLA-graphene films were micromachined using a femtosecond laser oscillator delivering 50-fs pulses and 800 nm, where the pulse energy and scanning speed was varied in order to determine the optimum irradiation parameters (16 of and 100 mu m/s) to the fabrication of microstructures. The micromachined patterns were characterized by optical microscopy and submitted to electrical measurements in liquid samples, clearly distinguishing all tastes tested. Our results confirm the femtosecond laser micromachining technique as an interesting approach to efficiently pattern PLA-graphene filaments with high precision and minimal mechanical defects, allowing the easy fabrication of interdigitated structures and an alternative method to those produced by conventional photolithography.

OPTICS AND LASER TECHNOLOGY 101, 74-79, 2017. DOI: 10.1016/j.optlastec.2017.11.006

[P042-2018] "Fiber taper diameter characterization using forward Brillouin scattering"

Jarschel, P. F.*; Magalhaes, L. S.*; Aldaya, I.*; Florez, O.*; Dainese, P.*

We propose a fast and non-destructive method to characterize the absolute diameter and uniformity of micrometer--scale fiber tapers using a pump and probe forward Brillouin scattering setup. The fundamental torsional-radial acoustic mode supported by the wire is excited using a pulsed pump laser and oscillates at a frequency that is inversely proportional to the taper waist diameter. This standing time-varying torsional-radial wave induces polarization modulation on a probe signal, whose spectrum structure reveals the sample diameter and its non-uniformity. By comparing our results with measurements using scanning-electron microscopy, a relative deviation of 1% or less was demonstrated, and diameter non-uniformity of less than 0.5% could be detected.

OPTICS LETTERS 43(5), 995-998, 2018. DOI: 10.1364/OL.43.000995

[P043-2018] "First measurement of jet mass in Pb-Pb and p-Pb collisions at the LHC"

Acharya, S.; Adamova, D.; Aggarwal, M. M.; **Albuquerque, D. S. D.*; Chinellato, D. D.*; De Souza, R. D.*; Takahashi, J.***; ALICE Collaboration

This letter presents the first measurement of jet mass in Pb--Pb and Pb-Pb collisions at root s(NN) = 2.76 TeV and root s(NN) = 5.02 TeV, respectively. Both the jet energy and the jet mass are expected to be sensitive to jet quenching in the hot Quantum Chromodynamics (QCD) matter created in nuclear collisions at collider energies. Jets are reconstructed from charged particles using the anti-k(T) jet algorithm and resolution parameter R = 0.4. The jets are measured in the pseudorapidity range |eta(jet)| < 0.5 and in three intervals of transverse momentum between 60 GeV/c and 120 GeV/c. The measurement of the jet mass in central Pb-Pb collisions is compared to the jet mass as measured in p-Pb reference collisions, to vacuum event generators, and to models including jet quenching. It is observed that the jet mass in central Pb-Pb collisions is consistent within uncertainties with p-Pb reference measurements. Furthermore, the measured jet mass in Pb-Pb collisions is not reproduced by the quenching models considered in this letter and is found to be consistent with PYTHIA expectations within systematic uncertainties.

PHYSICS LETTERS B 776, 249-264, 2018. DOI: 10.1016/j.physletb.2017.11.044

[P044-2018] "Fourier transform spectrometer on silicon with thermo-optic non-linearity and dispersion correction"

Souza, M. C. M. M.*; Grieco, A.; **Frateschi, N. C.***; Fainman, Y.

Miniaturized integrated spectrometers will have unprecedented impact on applications ranging from unmanned aerial vehicles to mobile phones, and silicon photonics promises to deliver compact, cost-effective devices. Mirroring its ubiquitous free-space counterpart, a silicon photonics-based Fourier transform spectrometer (Si-FTS) can bring broadband operation and fine resolution to the chip scale. Here we present the modeling and experimental demonstration of a thermally tuned Si-FTS accounting for dispersion, thermo--optic non-linearity, and thermal expansion. We show how these effects modify the relation between the spectrum and interferogram of a light source and we develop a quantitative correction procedure through calibration with a tunable laser. We retrieve a broadband spectrum (7 THz around 193.4 THz with 0.38-THz resolution consuming 2.5W per heater) and demonstrate the Si-FTS resilience to fabrication variations - a major advantage for large-scale manufacturing. Providing design flexibility and robustness, the Si-FTS is poised to become a fundamental building block for on-chip spectroscopy.

NATURE COMMUNICATIONS 9, 665, 2018. DOI: 10.1038/s41467-018-03004-6

[P045-2018] "Inclusive Search for a Highly Boosted Higgs Boson Decaying to a Bottom Quark-Antiquark Pair"

Sirunyan, A. M.; Tumasyan, A.; Adam, W.; **Chinellato, J. A.*; Tonelli Manganote, E. J.***; et al.
CMS Collaboration

An inclusive search for the standard model Higgs boson (H) produced with large transverse momentum (p(T)) and decaying to a bottom quark-antiquark pair (b (b) over bar) is performed using a data set of pp collisions at root s = 13 TeV collected with the CMS experiment at the LHC. The data sample corresponds to an integrated luminosity of 35.9 fb(-1). A highly Lorentz-boosted Higgs boson decaying to b (b) over bar is reconstructed as a single, large radius jet and is identified using jet substructure and dedicated b tagging techniques. The method is validated with Z -> b (b) over bar decays. The Z -> b (b) over bar process is observed for the first time in the single-jet topology with a local significance of 5.1 standard deviations (5.8 expected). For a Higgs boson mass of 125 GeV, an excess of events above the expected background is observed (expected) with a local significance of 1.5 (0.7) standard deviations. The measured cross section times branching fraction for production via gluon fusion of H -> b (b) over bar with p(T) > 450 GeV and in the pseudorapidity range -2.5 <eta< 2.5 is 74 +/- 48 (stat)(-10)(+17) (syst) fb, which is consistent within uncertainties with the standard model prediction.

PHYSICAL REVIEW LETTERS 120(7), 071802, 2018. DOI: 10.1103/PhysRevLett.120.071802

[P046-2018] "Influence of Deposition Conditions on the Characteristics of Luminescent Silicon Carbonitride Thin Films"

Khatami, Z.; **Bosco, G. B. F.***; Wojcik, J.; **Tessler, L. R.***; Mascher, P.

The influence of the substrate temperature and argon gas flow on the compositional, structural, optical, and light emission properties of amorphous hydrogenated silicon carbonitride (a-SiCxNy: H) thin films were studied. Thin films were fabricated using electron cyclotron resonance plasma enhanced chemical vapor deposition (ECR PECVD) at a range of substrate temperatures from 120 to 170 degrees C (corresponding to deposition temperatures of 300 to 450 degrees C) in a mixture of SiH4, N-2, and CH4 precursors. Variable angle spectroscopic ellipsometer (VASE), elastic recoil detection (ERD), and Rutherford backscattering spectrometry (RBS) verified optical bandgap widening, layer densification, and an increase of the refractive index at higher substrate temperatures. The microstructure of a-SiCxNy: H-z thin films was determined by X-ray photoelectron spectroscopy (XPS) and Fourier transform infrared (FTIR) spectroscopy. The substrate temperature strongly affected the binding state of all atoms, and in particular, carbon atoms attached to silicon and nitrogen, as well as hydrogen-terminated bonds. We correlated the films' microstructural changes to a higher species' mobility arriving on the growin layer at higher temperatures. Photoluminescence (PL) measurements showed that the total intensity of visible light emission increased. A systematic blueshift of the centroid of the wide PL peak was observed following the increase of optical gap.

ECS JOURNAL OF SOLID STATE SCIENCE AND TECHNOLOGY 7(2) N7-N14, 2018. DOI: 10.1149/2.0151802jss

[P047-2018] "J/psi production as a function of charged--particle pseudorapidity density in p-Pb collisions at root s(NN)=5.02 TeV"

Adamova, D.; Aggarwal, M. M.; Rinella, G. Aglieri; **Albuquerque, D. S. D.*; Chinellato, D. D.*; De Souza, R. D.*; Takahashi, J.***; et al.
ALICE Collaboration

We report measurements of the inclusive J/psi yield and average transverse momentum as a function of charged-particle pseudorapidity density dNch/d.in p-Pb collisions at root s(NN)= 5.02 TeVwith ALICE at the LHC. The observables are normalised to their corresponding averages in non-single diffractive events. An increase of the normalised J/psi yield with normalised dN(ch)/d(eta), measured at mid-rapidity, is observed at mid-rapidity and backward rapidity. At forward rapidity, a saturation of the relative yield is observed for high charged-particle multiplicities. The normalised average transverse momentum at forward and backward rapidities increases with multiplicity at low multiplicities and saturates beyond moderate multiplicities. In addition, the forward-to-backward nuclear modification factor ratio is also reported, showing an increasing suppression of J/psi production at forward rapidity with respect to backward rapidity for increasing charged-particle multiplicity.

PHYSICS LETTERS B 776, 91-104, 2018. DOI: 10.1016/j.physletb.2017.11.008

[P048-2018] "Lattice dynamics of ASb(2)O(6) (A = Cu, Co) with trirutile structure"

Maimone, D. T.*; Christian, A. B.; Neumeier, J. J.; **Granado, E.***

Raman spectroscopy experiments on single crystals of CuSb2O6 and CoSb2O6 quasi-one-dimensional antiferromagnets with trirutile crystal structure were performed, with a focus on the first material. The observed Raman-active phonon modes and previously reported infrared-active modes were identified with the aid of ab initio lattice dynamics calculations. The structural transition between monoclinic beta-CuSb2O6 and tetragonal alpha-CuSb2O6 phases at T-s = 400 K is manifested in our spectra by a "repulsion" of two accidentally quasidegenerate symmetric modes below T-s, caused by a phonon mixing effect that is only operative in the monoclinic beta-CuSb2O6 phase due to symmetry restrictions. Also, two specific phonons, associated with CuO6

octahedra rotation and with a Jahn-Teller elongation mode, soften and broaden appreciably as T -> T-s. A crossover from a displacive to an order-disorder transition at T-s is inferred.

PHYSICAL REVIEW B 97(10), 104304, 2018. DOI: 10.1103/PhysRevB.97.104304

[P049-2018] "Magnetotransport properties in the magnetic phase of BaFeAs (= Co,Ni): A magnetic excitations approach"

Pena, J. P.; **Piva, M. M.*; Rosa, P. F. S.*; Pagliuso, P. G.*; Adriano, C.***; Grant, T.; Fisk, Z.; Baggio-Saitovitch, E.; Pureur, P.

Because of their complex Fermi surfaces, the identification of the physical phenomena contributing to electronic scattering in the Fe-based superconductors is a difficult task. Here, we report on the electrical resistivity, magnetoresistance, and Hall effect in two series of BaFe2-xTxAs2 (T = Co, Ni) crystals with different values of x. The T contents were chosen so that the majority of the investigated samples present an intermediate magnetically ordered state and a superconducting ground state. We interpret the obtained results in terms of scattering of charge carriers by magnetic excitations instead of describing them as resulting uniquely from effects related to multiple-band conduction. Our samples are single crystals from the structural point of view and their overall magnetotransport properties are dominated by a single magnetic state.

PHYSICAL REVIEW B 97(10), 104502, DOI: 10.1103/PhysRevB.97.104502

[P050-2018] "Measurements of t(t)over-bar cross sections in association with b jets and inclusive jets and their ratio using dilepton final states in pp collisions at root s=13 TeV"

Sirunyan, A. M.; Tumasyan, A.; Adam, W.; **Chinellato, J. A.*; Tonelli Manganote, E. J.***; et al.
CMS Collaboration

The cross sections for the production of t (t) over bar b (b) over bar and t (t) over bar jj events and their ratio sigma(t (t) over bar b (b) over bar)/sigma(t (t) over bar jj) are measured using data corresponding to an integrated luminosity of 2.3 fb(-1) collected in pp collisions at root s = 13 TeV with the CMS detector at the LHC. Events with two leptons (e or mu) and at least four reconstructed jets, including at least two identified as b quark jets, in the final state are selected. In the full phase space, the measured ratio is 0.022 +/- 0.003 (stat) +/- 0.006 (syst), the cross section sigma(t (t) over bar b (b) over bar) bis 4.0 +/- 0.6 (stat)+/- 1.3 (syst) pb and sigma(t (t) over bar jj) is 184 +/- 6 (stat)+/- 33 (syst) pb. The measurements are compared with the standard model expectations obtained from a POWHEG simulation at next-to-leading-order interfaced with PYTHIA.

PHYSICS LETTERS B 776, 355-378, 2018. DOI: 10.1016/j.physletb.2017.11.043

[P051-2018] "Measurements of the pp -> ZZ production cross section and the Z -> 4l branching fraction, and constraints on anomalous triple gauge couplings at root s=13TeV"

Sirunyan, A. M.; Tumasyan, A.; Adam, W.; **Chinellato, J. A.*; Tonelli Manganote, E. J.***; et al.
CMS Collaboration

Four-lepton production in proton-proton collisions, pp -> (Z/gamma*)(Z/gamma*) -> 4l, where l = e or mu, is studied at a center-of-mass energy of 13 TeV with the CMS detector at the LHC. The data sample corresponds to an integrated luminosity of 35.9 fb(-1). The ZZ production cross section, sigma(pp -> ZZ) = 17.2 +/- 0.5 (stat) +/- 0.7 (syst) +/- 0.4 (theo) +/- 0.4 (lumi) pb, measured using events with two opposite-sign, same-flavor lepton pairs produced in the mass region 60 < m(l+l-) < 120 GeV, is consistent with standard model predictions. Differential cross sections are measured and are well described by the theoretical predictions. The Z boson branching fraction to four leptons is measured to be B(Z -> 4l) = 4.83(-0.22)(+0.23) (stat)(-0.29)(+0.32) (syst) +/- 0.08 (theo) +/- 0.12(lumi) x 10(-6) for events with a four-lepton invariant mass in the range 80 < m(4l) < 100 GeV and a dilepton mass m(ll) > 4GeV for all opposite-sign, same-flavor lepton pairs. The results agree with standard model predictions. The invariant mass distribution of the four-lepton system is used to set limits on anomalous ZZZ and ZZ. couplings at 95% confidence level: -0.0012 < f(4)(Z) < 0.0010, -0.0010 < f(5)(Z) < 0.0013, -0.0012 < f(4)(gamma) < 0.0013, -0.0012 < f(5)(gamma) < 0.0013.

EUROPEAN PHYSICAL JOURNAL C 78(2), 165, DOI: 10.1140/epjc/s10052-018-5567-9

[P052-2018] "Novel event classification based on spectral analysis of scintillation waveforms in Double Chooz"

Abrahao, T.; Almazan, H.; dos Anjos, J. C.; **Gonzalez, L. F. G.*; Kemp, E.***; et al.
The Double Chooz collaboration

Liquid scintillators are a common choice for neutrino physics experiments, but their capabilities to perform background rejection by scintillation pulse shape discrimination is generally limited in large detectors. This paper describes a novel approach for a pulse shape based event classification developed in the context of the Double Chooz reactor antineutrino experiment. Unlike previous implementations, this method uses the Fourier power spectra of the scintillation pulse shapes to obtain event-wise information. A classification variable built from spectral information was able to achieve an unprecedented performance, despite the lack of optimization at the detector design level. Several examples of event classification are provided, ranging from differentiation between the detector volumes and an efficient rejection of instrumental light noise, to some sensitivity to the particle type, such as stopping muons, ortho-positronium formation, alpha particles as well as electrons and positrons. In combination with other techniques the method is expected to allow for a versatile and more efficient background rejection in the future, especially if detector optimization is taken into account at the design level.

JOURNAL OF INSTRUMENTATION 13, P01031, 2018. DOI: 10.1088/1748-0221/13/01/P01031

[P053-2018] "Observation of Correlated Azimuthal Anisotropy Fourier Harmonics in pp and p plus Pb Collisions at the LHC"

Sirunyan, A. M.; Tumasyan, A.; Adam, W.; **Chinellato, J. A.*; Tonelli Manganote, E. J.***; et al.
CMS Collaboration

The azimuthal anisotropy Fourier coefficients (v(n)) in 8.16 TeV p + Pb data are extracted via long-range two-particle correlations as a function of the event multiplicity and compared to corresponding results in pp and PbPb collisions. Using a four-particle cumulant technique, v(n) correlations are measured for the first time in pp and p + Pb collisions. The v(2) and v(4) coefficients are found to be positively correlated in all collision systems. For high-multiplicity p + Pb collisions, an anticorrelation of v(2) and v(3) is observed, with a similar correlation strength as in PbPb data at the same multiplicity. The new correlation results strengthen the case for a common origin of the collectivity seen in p + Pb and PbPb collisions in the measured multiplicity range.

PHYSICAL REVIEW LETTERS 120(9), 092301, 2018. DOI: 10.1103/PhysRevLett.120.092301

[P054-2018] "Observation of Electroweak Production of Same-Sign W Boson Pairs in the Two Jet and Two Same-Sign Lepton Final State in Proton-Proton Collisions at root s=13 TeV"

Sirunyan, A. M.; Tumasyan, A.; Adam, W.; **Chinellato, J. A*; Tonelli Manganote, E. J.***; et al.
CMS Collaboration

The first observation of electroweak production of same-sign W boson pairs in proton-proton collisions is reported. The data sample corresponds to an integrated luminosity of 35.9 fb(-1) collected at a center-of-mass energy of 13 TeV with the CMS detector at the LHC. Events are selected by requiring exactly two leptons (electrons or muons) of the same charge, moderate missing transverse momentum, and two jets with a large rapidity separation and a large dijet mass. The observed significance of the signal is 5.5 standard deviations, where a significance of 5.7 standard deviations is expected based on the standard model. The ratio of measured event yields to that expected from the standard model at leading order is 0.90 +/- 0.22. A cross section measurement in a fiducial region is reported. Bounds are given on the structure of quartic vector boson interactions in the framework of dimension-8 effective field theory operators and on the production of doubly charged Higgs bosons.

PHYSICAL REVIEW LETTERS 120(8), 081801, 2018. DOI: 10.1103/PhysRevLett.120.081801

[P055-2018] "On hardening silver nanocubes by high-velocity impacts: a fully atomistic molecular dynamics investigation"

Oliveira, E. F.*; Autreto, P. A. S.*; Galvo, D. S.*

Gradient nanograins (GNG) creation in metals has been a promising approach to obtain ultra-strong materials. Recently, R. Thevamaran et al. (Science 354:312 in 2016) proposed a single-step method based on high-velocity impacts of silver nanocubes (SNC) to produce almost perfect GNG. However, after certain time, these grains spontaneously coalesce, which compromises the induced hardening and other mechanical properties. To better understand these processes, a detailed investigation at the atomic scale of the deformation/hardening mechanisms are needed, which is one of the objectives of the present work. We carried out fully atomistic molecular dynamics (MD) simulations of silver nanocubes at high impact velocity values using realistic structural models. Our MD results suggest that besides the GNG mechanisms, the observed SNC hardening could be also the result of the existence of polycrystalline arrangements formed by HCP domains encapsulated by FCC ones in the smashed SNC. This can be a new way to design ultra-strong materials, even in the absence of GNG domains.

JOURNAL OF MATERIALS SCIENCE 53(10), 7486-7492, 2018. DOI: 10.1007/s10853-018-2104-z

[P056-2018] "Optical weak measurements without removing the Goos-Hanchen phase"

Araujo, M. P.*; De Leo, S.; **Maia, G. G.***

Optical weak measurements are a powerful tool for measuring small shifts of optical paths. When applied to the measurement of the Goos-Hanchen shift, in particular, a special step must be added to its protocol: the removal of the relative Goos-Hanchen phase, since its presence generates a destructive influence on the measurement. There is, however, a lack of description in the literature of the precise effect of the Goos-Hanchen phase on weak measurements. In this paper we address this issue, developing an analytic study for a Gaussian beam transmitted through a dielectric structure. We obtain analytic expressions for weak measurements as a function of the relative Goos-Hanchen phase and show how to remove it without the aid of waveplates.

JOURNAL OF MODERN OPTICS 65(7), 837-846, 2018. DOI: 10.1080/09500340.2017.1404654

[P057-2018] "Pd Nanoparticles Immobilized on Graphene Oxide/Silica Nanocomposite: Efficient and Recyclable Catalysts for Cross-Coupling Reactions"

Oliveira, R. L.; Oliveira, C. S.; **Landers, R.*;** Correia, C. R. D.

Pd nanoparticles were synthesized on non-functionalized and functionalized graphene oxide with thiol and amine groups. The resulting materials were used as recyclable catalysts to study the influence of the functional groups and compare their activity and stability to non-functionalized graphene oxide and commercial catalysts in the Heck and Suzuki reactions. The catalyst based on non-functionalized GO and commercial catalysts lost their activity quickly because of particle growth (Oswald ripening). However, the presence of functional groups reduces significantly the metal particle growth producing more efficient catalysts for the Heck and the Suzuki reactions. Moreover, the synthesized catalysts were capable of catalyzing the Heck and Suzuki reactions using different substrates, achieving good activities and selectivities in all cases.

CHEMISTRYSELECT 3(2), 535-543, 2018. DOI: 10.1002/slct.201702693

[P058-2018] "Perovskite Thin Film Synthesised from Sputtered Lead Sulphide"

da Silva, J. C. M.*; Ermakov, V. A.*; Marques, F. C.*

In the last few years, research on dye-sensitised devices has been focused on the development of solar cells, based on CH3NH3PbX3 (X = I-, Br-, Cl-) composites with perovskite structure. The deposition of perovskite thin films is usually carried out by solution-based processes using spincoating techniques that result in the production of high quality films. Solar cells made by this method exceed 20% efficiency, with the potential for use in large scale production through ink print or screen printing techniques. As an alternative route, perovskite thin films can be deposited through thermal evaporation. A new method is proposed to produce CH3NH3PbI3, based on a radio-frequency (rf) -sputtering technique that results in a high reproducibility of the films and is compatible with roll-toroll processes. We deposited thin films of lead-sulphide (PbS) and converted them into perovskite by placing the films in an iodine atmosphere, followed by dipping in a solution of methylammonium iodide (CH3NH3I). The conversions to PbI2 and CH3NH3PbI3 were confirmed by elemental analyses, absorption, and photoluminescence spectroscopy. Structural properties were revealed by X-ray diffraction and infrared and Raman spectroscopy.

SCIENTIFIC REPORTS 8, 1563, 2017. DOI: 10.1038/s41598-018-19746-8

[P059-2018] "Phase collapse and revival of a 1-mode Bose--Einstein condensate induced by an off-resonant optical probe field and superselection rules"

Arruda, L. G. E.; Prataviera, G. A.; **de Oliveira, M. C.***

Phase collapse and revival for Bose-Einstein condensates are non-linear phenomena appearing due to atomic collisions. While it has been observed in a general setting involving many modes, for one-mode condensates its occurrence is forbidden by the particle number superselection rule (SSR), which arises because there is no phase reference available.

We consider a single mode atomic Bose-Einstein condensate interacting with an off-resonant optical probe field. We show that the condensate phase revival time is dependent on the atom-light interaction, allowing optical control on the atomic collapse and revival dynamics. Incoherent effects over the condensate phase are included by considering a continuous photo--detection over the probe field. We consider conditioned and unconditioned photo-counting events and verify that no extra control upon the condensate is achieved by the probe photo detection, while further inference of the atomic system statistics is allowed leading to a useful test of the SSR on particle number and its imposition on the kind of physical condensate state.

ANNALS OF PHYSICS 389, 30-47, 2018. DOI: 10.1016/j.aop.2017.11.016

[P060-2018] "Plasma immersion ion implantation (PIII) influence on Ti-6Al-4V alloy: Frequency effect"

Oliveira, V. M. C. A.; Cioffi, M. O. H.; Barboza, M. J. R.; **Landers, R.***; Schmitt, B.; Tapia, D. C. A. R.; Voorwald, H. J. C.

The plasma immersion ion implantation treatment (PIII) acts to increase mechanical resistance with solid solution formation, new phases and defects inclusion, besides chemical and residual stress profile modification. Ti-6Al-4V alloy presents poor tribological properties and high affinity with interstitial elements, such as nitrogen and oxygen, this makes it more reactive at high temperatures. This paper aims to study Ti-6Al-4V alloy fatigue behavior subjected to nitrogen addition by plasma immersion ion implantation. It was investigated the frequency parameter influence on fatigue resistance. Ti-6Al-4V alloy was PIII treated with voltage equal to 9.5 kV, frequencies varying between 1000 and 1500 Hz and submitted to axial fatigue tests. Axial fatigue tests were performed, at room temperature and R = 0.1. Ti-6Al-4V alloy fatigue results were supported by Weibull statistics analysis. Ti-6Al-4V alloy microstructural analysis showed equiaxed alpha + beta grains. Weibull analysis at untreated condition presented m values greater than 1, indicating reliability and uniformity. For a lifetime of 10(7) cycles, fatigue resistance was equal to 829 MPa for untreated condition, 644, 767 and 417 MPa, for f = 1000, 1200 and 1500 Hz, respectively. The nitrogen-based compounds were detected only at the condition where f = 1200 Hz. Thus, the combination of PIII treatment parameters, when f = 1200 Hz, hindered crack nucleation and increasing fatigue resistance of treated Ti-6Al-4V alloy when compared with the other two treatment conditions.

INTERNATIONAL JOURNAL OF FATIGUE 109, 157-165, 2018. DOI: 10.1016/j.ijfatigue.2017.12.016

[P061-2018] "Predicting Ligand-Free Cell Attachment on Next-Generation Cellulose-Chitosan Hydrogels"

Johns, M. A.; Bae, Y.; Guimaraes, F. E. G.; Lanzoni, E. M.; Costa, C. A. R.; Murray, P. M.; **Deneke, C.***; Galembeck, F.; Scott, J. L.; Sharma, R. I.

There is a growing appreciation that engineered biointerfaces can regulate cell behaviors, or functions. Most systems aim to mimic the cell-friendly extracellular matrix environment and incorporate protein ligands; however, the understanding of how a ligand-free system can achieve this is limited. Cell scaffold materials comprised of interfused chitosan-cellulose hydrogels promote cell attachment in ligand-free systems, and we demonstrate the role of cellulose molecular weight, MW, and chitosan content and MW in controlling material properties and thus regulating cell attachment. Semi-interpenetrating network (SIPN) gels, generated from cellulose/ionic liquid/cosolvent solutions, using chitosan solutions as phase inversion solvents, were stable and obviated the need for chemical coupling. Interface properties, including surface zeta-potential, dielectric constant, surface roughness, and shear modulus, were modified by varying the chitosan degree of polymerization and solution concentration, as well as the source of cellulose, creating a family of cellulose-chitosan SIPN materials. These features, in turn, affect cell attachment onto the hydrogels and the utility of this ligand-free approach is extended by forecasting cell attachment using regression modeling to isolate the effects of individual parameters in an initially complex system. We demonstrate that increasing the charge density, and/or shear modulus, of the hydrogel results in increased cell attachment.

ACS OMEGA 3(1), 937-945, 2018. DOI: 10.1021/acsomega.7b01583

[P062-2018] "Production of deuterons, tritons, He-3 nuclei, and their antinuclei in pp collisions at root s=0.9, 2.76, and 7 TeV"

Acharya, S.; Adam, J.; Adamova, D.; **Albuquerque, D. S. D.*; Chinellato, D. D.*; De Souza, R. D.*; Takahashi, J.***; et al.
ALICE Collaboration

Invariant differential yields of deuterons and antideuterons in pp collisions at root s = 0.9, 2.76 and 7 TeV and the yields of tritons, He-3 nuclei, and their antinuclei at root s = 7 TeV have been measured with the ALICE detector at the CERN Large Hadron Collider. The measurements cover a wide transverse momentum (p(T)) range in the rapidity interval vertical bar y vertical bar < 0.5, extending both the energy and the pT reach of previous measurements up to 3 GeV/c for A = 2 and 6 GeV/c for A = 3. The coalescence parameters of (anti) deuterons and 3 He nuclei exhibit an increasing trend with pT and are found to be compatible with measurements in pA collisions at low p(T) and lower energies. The integrated yields decrease by a factor of about 1000 for each increase of the mass number with one (anti) nucleon. Furthermore, the deuteron--to-proton ratio is reported as a function of the average charged particle multiplicity at different center-of-mass energies.

PHYSICAL REVIEW C 97(2), 024615, 2018. DOI: 10.1103/PhysRevC.97.024615

[P063-2018] "Pseudorapidity distributions of charged hadrons in proton-lead collisions at root s(NN)=5:02 and 8.16 TeV"

Sirunyan, A. M.; Tumasyan, A.; Adam, W.; **Chinellato, J. A.*; Tonelli Manganote, E. J.***; et al.
CMS Collaboration

The pseudorapidity distributions of charged hadrons in proton--lead collisions at nucleon-nucleon center-of-mass energies root s(NN) = 5.02 and 8.16 TeV are presented. The measurements are based on data samples collected by the CMS experiment at the LHC. The number of primary charged hadrons produced in non-single-diffractive proton-lead collisions is determined in the pseudorapidity range vertical bar eta(lab)vertical bar < 2.4. The charged-hadron multiplicity distributions are compared to the predictions from theoretical calculations and Monte Carlo event generators. In the center-of-mass pseudorapidity range vertical bar eta(cm)vertical bar < 0.5, the average charged-hadron multiplicity densities < dN(ch)/d eta(cm)>vertical bar(vertical bar eta cm vertical bar) < 0.5 are 17.1 +/- 0.01 (stat) +/- 0.59 (syst) and 20.10 +/- 0.01 (stat) +/- 0.5(syst) at root s(NN) = 5.02 and 8.16 TeV, respectively. The particle densities per participant nucleon are compared to similar measurements in proton-proton, proton-nucleus, and nucleus-nucleus collisions.

JOURNAL OF HIGH ENERGY PHYSICS 1, 045, 2018. DOI: 10.1007/JHEP01(2018)045

[P064-2018] "Red-Emitting Magnetic Nanocomposites Assembled from Ag-Decorated Fe3O4@SiO2 and Y2O3:Eu3+: Impact of Iron-Oxide/Silver Nanoparticles on Eu3+ Emission"

Khan, L. U.; Zambon, L. F. M.; Santos, J. L.; Rodrigues, R. V.; Costa, L. S.; **Muraca, D.*; Pirota, K. R.***; Felinto, M. C. F. C.; Malta, O. L.; Brito, H. F.

The new multistep approach for co-assembling magnetic iron oxide nanoflowers with red-emitting Y2O3:Eu3+ to form luminescent and magnetic nanocomposites was reported. The Fe3O4 core prepared by solvothermal method was layered by SiO2 shell and decorated with small size spherical Ag nanoparticles as well as further coated with Y2O3:Eu3+ luminophore. The nanoflower shape Fe3O4 core of size similar to 110 nm and crystalline cubic structure of bifunctional iron-oxide@ Y2O3:Eu3+, Fe3O4@SiO2@Y2O3:Eu3+ and Fe3O4@SiO2-Ag@ Y2O3:Eu3+ (1 mol%) nanomaterials were confirmed from X-rays diffraction, EDS spectra and transmission electron microscopy (TEM) images. The static magnetic measurements supported and manifested nonsuperparamagnetic behavior of the materials at 300 K. The iron oxides are usually luminescence quenchers. In order to rationalize this effect, their optical properties based on their emission spectral data and luminescence decay curves were studied. Experimental intensity parameters (Wl), lifetimes (t), intrinsic quantum yield (Q(Ln)(Ln)) as well as radiative (Arad) and non-radiative (Anrad) decay rates were calculated to probe the local chemical environment of the Eu3+ ion and to better understand the phenomena of iron oxide induced luminescence quenching. The highest value of the intrinsic quantum yield (Q(Ln)(Ln) = 74%) for the alpha-Fe2O3@ Y2O3:Eu3+ (1 mol%) among all the luminescent and magnetic nanocomposites suggests that alpha-Fe2O3 phase induces a lower luminescence quenching then Fe3O4/g-Fe2O3. The SiO2 thin layer leads to improve the luminescence efficiency, whereas the Ag nanoparticles act as luminescence quencher. These novel Eu3+ nanomaterials may act as a red emitting layer for magnetic and light converting molecular devices.

CHEMISTRYSELECT 3(4), 1157-1167, 2018. DOI: 10.1002/slct.201702478

[P065-2018] "Ripplocation in graphite nanoplatelets during sonication assisted liquid phase exfoliation"

Alaferdov, A. V.; Savu, R.; Canesqui, M. A.; **Kopelevich, Y. V.*; da Silva, R. R.***; Rozhkova, N. N.; Pavlov, D. A.; Usov, Yu. V.; de Trindade, G. M.; Moshkalev, S. A.

Defects induced by liquid-phase exfoliation of graphite using sonication were studied. It was shown that localized impact by cavitation shock waves can produce bulk ripplocations and various types of dislocations in graphite nanoplatelets. Formation of ripples is more pronounced in large aspect (length/width) ratio platelets or nanobelts. Quasi-periodical ripple systems were observed in many nanobelts after sonication. Mechanism of formation of ripples and dislocations during sonication was proposed. Surprisingly, fast high-temperature processing was found to anneal most of defects. This is consistent with our observations that defects associated with ripplocations are strongly localized and thus can be fast annealed.

CARBON 129, 826-829, 2018. DOI: 10.1016/j.carbon.2017.12.100

[P066-2018] "Robust nanofabrication of monolayer MoS2 islands with strong photoluminescence enhancement via local anodic oxidation"

Fernandes, T. F. D.; Gadelha, A. C.; Barboza, A. P. M.; Paniago, R. M.; Campos, L. C.; Guimaraes, P. S. S.; **de Assis, P. L.***; Neves, B. R. A.

In this work, we demonstrate the nanofabrication of monolayer MoS2 islands using local anodic oxidation of few-layer and bulk MoS2 flakes. The nanofabricated islands present true monolayer Raman signal and photoluminescence intensity up to two orders of magnitude larger than that of a pristine monolayer. This technique is robust enough to result in monolayer islands without the need of meticulously fine-tuning the oxidation process, thus providing a fast and reliable way of creating monolayer regions with enhanced optical properties and with controllable size, shape, and position.

2D MATERIALS 5(2), 025018, 2018. DOI: 10.1088/2053-1583/aab38c

[P067-2018] "Search for heavy resonances decaying to a top quark and a bottom quark in the lepton plus jets final state in proton-proton collisions at 13 TeV"

Sirunyan, A. M.; Tumasyan, A.; Adam, W.; **Chinellato, J. A.*; Tonelli Manganote, E. J.***; et al.
CMS Collaboration

A search is presented for narrow heavy resonances decaying to a top quark and a bottom quark using data collected by the CMS experiment at root s= 13 TeV in 2016. The data set analyzed corresponds to an integrated luminosity of 35.9fb(-1). Final states that include a single lepton (e, mu), multiple jets, and missing transverse momentum are analyzed. No evidence is found for the production of a W' boson, and the production of right-handed W' bosons is excluded at 95% confidence level for masses up to 3.6 TeV depending on the scenario considered. Exclusion limits for W' bosons are also presented as a function of their coupling strength to left- and right-handed fermions. These limits on a W' boson decaying via a top and a bottom quark are the most stringent published to date.

PHYSICS LETTERS B 777, 39-63, 2018. DOI: 10.1016/j.physletb.2017.12.006

[P068-2018] "Search for Higgs boson pair production in events with two bottom quarks and two tau leptons in proton-proton collisions at root s=13 TeV"

Sirunyan, A. M.; Tumasyan, A.; Adam, W.; **Chinellato, J. A.*; Tonelli Manganote, E. J.***; et al.
CMS Collaboration

A search for the production of Higgs boson pairs in proton-proton collisions at a centre-of-mass energy of 13TeVis presented, using a data sample corresponding to an integrated luminosity of 35.9fb(-1) collected with the CMS detector at the LHC. Events with one Higgs boson decaying into two bottom quarks and the other decaying into two tau leptons are explored to investigate both resonant and nonresonant production mechanisms. The data are found to be consistent, within uncertainties, with the standard model background predictions. For resonant production, upper limits at the 95% confidence level are set on the production cross section for Higgs boson pairs as a function of the hypothesized resonance mass and are interpreted in the context of the minimal supersymmetric standard model. For nonresonant production, upper limits on the production cross section constrain the parameter space for anomalous Higgs boson couplings. The observed (expected) upper limit at 95% confidence level corresponds to about 30(25) times the prediction of the standard model.

PHYSICS LETTERS B 778, 101-127, 2018. DOI: 10.1016/j.physletb.2018.01.001

[P069-2018] "Search for Higgsino pair production in pp collisions at root s=13 TeV in final states with large missing transverse momentum and two Higgs bosons decaying via H -> b(b)over bar"

Sirunyan, A. M.; Tumasyan, A.; Adam, W.; **Chinellato, J. A.*; Tonelli Manganote, E. J.*;** et al.
CMS Collaboration

Results are reported from a search for new physics in 13 TeV proton-proton collisions in the final state with large missing transverse momentum and two Higgs bosons decaying via H -> b(b)over bar. The search uses a data sample accumulated by the CMS experiment at the LHC in 2016, corresponding to an integrated luminosity of 35.9 fb(-1). The search is motivated by models based on gauge-mediated supersymmetry breaking, which predict the electroweak production of a pair of Higgsinos, each of which can decay via a cascade process to a Higgs boson and an undetected lightest supersymmetric particle. The observed event yields in the signal regions are consistent with the standard model background expectation obtained from control regions in data. Higgsinos in the mass range 230-770 GeV are excluded at 95% confidence level in the context of a simplified model for the production and decay of approximately degenerate Higgsinos.

PHYSICAL REVIEW D 97(3), 032007, 2018. DOI: 10.1103/PhysRevD.97.032007

[P070-2018] "Search for low mass vector resonances decaying into quark-antiquark pairs in proton-proton collisions at root s=13 TeV"

Sirunyan, A. M.; Tumasyan, A.; Adam, W.; **Chinellato, J. A.*; Tonelli Manganote, E. J.***; et al.
CMS Collaboration

A search for narrow vector resonances decaying into quark--antiquark pairs is presented. The analysis is based on data collected in proton-proton collisions at root s = 13 TeV with the CMS detector at the LHC, corresponding to an integrated luminosity of 35.9 fb(-1). The hypothetical resonance is produced with sufficiently high transverse momentum that its decay products are merged into a single jet with two-prong substructure. A signal would be identified as a peak over a smoothly falling background in the distribution of the invariant mass of the jet, using novel jet substructure techniques. No evidence for such a resonance is observed within the mass range of 50-300 GeV. Upper limits at 95% confidence level are set on the production cross section, and presented in a mass--coupling parameter space. The limits further constrain simplified models of dark matter production involving a mediator interacting between quarks and dark matter particles through a vector or axial-vector current. In the framework of these models, the results are the most sensitive to date, extending for the first time the search region to masses below 100 GeV.

JOURNAL OF HIGH ENERGY PHYSICS 1, 097, 2018. DOI: 10.1007/JHEP01(2018)097

[P071-2018] "Search for pair production of excited top quarks in the lepton plus jets final state The CMS Collaboration"

Sirunyan, A. M.; Tumasyan, A.; Adam, W.; **Chinellato, J. A.*; Tonelli Manganote, E. J.***; et al.
CMS Collaboration

A search is performed for the pair production of spin-3/2 excited top quarks, each decaying to a top quark and a gluon. The search uses the data collected with the CMS detector from proton-proton collisions at a center-of-mass energy of 13 TeV, corresponding to an integrated luminosity of 35.9 fb(-1). Events are selected by requiring an isolated muon or electron, an imbalance in the transverse momentum, and at least six jets of which exactly two must be compatible with originating from the fragmentation of a bottom quark. No significant excess over the standard model predictions is found. A lower limit of 1.2 TeV is set at 95% confidence level on the mass of the spin-3/2 excited top quark in an extension of the Randall--Sundrum model, assuming a 100% branching fraction of its decay into a top quark and a gluon. These are the best limits to date in a search for excited top quarks and the first at 13 TeV.

PHYSICS LETTERS B 778, 349-370, 2018. DOI: 10.1016/j.physletb.2018.01.049

[P072-2018] "Search for standard model production of four top quarks with same-sign and multilepton final states in proton-proton collisions at root s=13TeV"

Sirunyan, A. M.; Tumasyan, A.; Adam, W.; **Chinellato, J. A.*; Tonelli Manganote, E. J.***; et al.
CMS Collaboration

A search for standard model production of four top quarks (t (t) over bart (t) over bar) is reported using events containing at least three leptons (e, mu) or a same-sign lepton pair. The events are produced in proton-proton collisions at a center--of-mass energy of 13 TeVat the LHC, and the data sample, recorded in 2016, corresponds to an integrated luminosity of 35.9 fb(-1). Jet multiplicity and flavor are used to enhance signal sensitivity, and dedicated control regions are used to constrain the dominant backgrounds. The observed and expected signal significances are, respectively, 1.6 and 1.0 standard deviations, and the t (t) over bart (t) over bar cross section ismeasured to be 16.9(-11.4)(+13.8) fb, in agreement with next-to-leading-order standard model predictions. These results are also used to constrain the Yukawa coupling between the top quark and the Higgs boson to be less than 2.1 times its expected standard model value at 95% confidence level.

EUROPEAN PHYSICAL JOURNAL C 78(2), 140, 2018. DOI: 10.1140/epjc/s10052-018-5607-5

[P073-2018] "Search for supersymmetry in events with at least three electrons or muons, jets, and missing transverse momentum in proton-proton collisions at root s=13 TeV"

Sirunyan, A. M.; Tumasyan, A.; Adam, W.; **Chinellato, J. A.*; Tonelli Manganote, E. J.***; et al.
CMS Collaboration

A search for new physics is carried out in events with at least three electrons or muons in any combination, jets, and missing transverse momentum. Results are based on the sample of proton-proton collision data produced by the LHC at a center-of-mass energy of 13TeV and collected by the CMS experiment in 2016. The data sample analyzed corresponds to an integrated luminosity of 35.9 fb(-1). Events are classified according to the number of b jets, missing transverse momentum, hadronic transverse momentum, and the invariant mass of same-flavor dilepton pairs with opposite charge. No significant excess above the expected standard model background is observed. Exclusion limits at 95% confidence level are computed for four different supersymmetric simplified models with pair production of gluinos or third-generation squarks. In the model with gluino pair production, with subsequent decays into a top quark-antiquark pair and a neutralino, gluinos with masses smaller than 1610 GeV are excluded for a massless lightest supersymmetric particle. In the case of bottom squark pair production, the bottom squark masses are excluded up to 840 GeV for charginos lighter than 200 GeV.

For a simplified model of heavy top squark pair production, the (t) over tilde (2) mass is excluded up to 720, 780, or 710 GeV for models with an exclusive (t) over tilde (2) -> (t) over tilde H-1 decay, an exclusive (t) over tilde (2) -> (t) over tilde (1)Z decay, or an equally probable mix of those two decays. In order to provide a simplified version of the analysis for easier interpretation, a small set of aggregate signal regions also has been de fined, providing a compromise between simplicity and analysis sensitivity.

JOURNAL OF HIGH ENERGY PHYSICS 2, 067, 2018. DOI: 10.1007/JHEP02(2018)067

[P074-2018] "Search for supersymmetry in proton-proton collisions at 13 TeV using identified top quarks"

Sirunyan, A. M.; Tumasyan, A.; Adam, W.; **Chinellato, J. A.*; Tonelli Manganote, E. J.***; et al.
CMS Collaboration

A search for supersymmetry is presented based on proton--proton collision events containing identified hadronically decaying top quarks, no leptons, and an imbalance p(T)(miss) in transverse momentum. The data were collected with the CMS detector at the CERN LHC at a center-of-mass energy of 13 TeV, and correspond to an integrated luminosity of 35.9 fb(-1). Search regions are defined in terms of the multiplicity of bottom quark jet and top quark candidates, the p(T)(miss) , the scalar sum of jet transverse momenta, and themT2 mass variable. No statistically significant excess of events is observed relative to the expectation from the standard model. Lower limits on the masses of supersymmetric particles are determined at 95% confidence level in the context of simplified models with top quark production. For a model with direct top squark pair production followed by the decay of each top squark to a top quark and a neutralino, top squark masses up to 1020 GeVand neutralino masses up to 430 GeVare excluded. For amodel with pair production of gluinos followed by the decay of each gluino to a top quark-antiquark pair and a neutralino, gluino masses up to 2040 GeVand neutralino masses up to 1150 GeVare excluded. These limits extend previous results.

PHYSICAL REVIEW D 97(1), 012007, 2018. DOI: 10.1103/PhysRevD.97.012007

[P075-2018] "Search for the pair production of third-generation squarks with two-body decays to a bottom or charm quark and a neutralino in proton-proton collisions at root s=13 TeV"

Sirunyan, A. M.; Tumasyan, A.; Adam, W.; **Chinellato, J. A.*; Tonelli Manganote, E. J.***; et al.
CMS Collaboration

Results are presented from a search for the pair production of third-generation squarks in proton-proton collision events with two-body decays to bottom or charm quarks and a neutralino, which produces a significant imbalance in the transverse momentum. The search is performed using a sample of proton--proton collision data at root s = 13 TeV recorded by the CMS experiment at the LHC, corresponding to an integrated luminosity of 35.9fb(-1). No statistically significant excess of events is observed beyond the expected contribution from standard model processes. Exclusion limits are set in the context of simplified models of bottom or top squark pair production. Models with bottom squark masses up to 1220 GeV are excluded at 95% confidence level for light neutralinos, and models with top squark masses of 510 GeV are excluded assuming that the mass splitting between the top squark and the neutralino is small.

PHYSICS LETTERS B 778, 263-291, 2018. DOI: 10.1016/j.physletb.2018.01.012

[P076-2018] "Search for ZZ resonances in the 2l2v final state in proton-proton collisions at 13 TeV"

Sirunyan, A. M.; Tumasyan, A.; Adam, W.; **Chinellato, J. A.*; Tonelli Manganote, E. J.***; et al.
CMS Collaboration

A search for heavy resonances decaying to a pair of Z bosons is performed using data collected with the CMS detector at the LHC. Events are selected by requiring two oppositely charged leptons (electrons or muons), consistent with the decay of a Z boson, and large missing transverse momentum, which is interpreted as arising from the decay of a second Z boson to two neutrinos. The analysis uses data from proton-proton collisions at a center-of-mass energy of 13 TeV, corresponding to an integrated luminosity of 35.9 fb(-1). The hypothesis of a spin-2 bulk graviton (X) decaying to a pair of Z bosons is examined for 600 <= m(X) <= 2500 GeV and upper limits at 95% confidence level are set on the product of the production cross section and branching fraction of X -> ZZ ranging from 100 to 4 fb. For bulk graviton models characterized by a curvature scale parameter (k) over tilde = 0.5 in the extra dimension, the region nix < 800 GeV is excluded, providing the most stringent limit reported to date. Variations of the model considering the possibility of a wide resonance produced exclusively via gluon--gluon fusion or q<(q)over bar> annihilation are also examined.

JOURNAL OF HIGH ENERGY PHYSICS 3, 003, 2018. DOI: 10.1007/JHEP03(2018)003

[P077-2018] "Self-organized nickel nanoparticles on nanostructured silicon substrate intermediated by a titanium oxynitride (TiNxOy) interface"

Morales, M.*; Droppa, R., Jr.; de Mello, S. R. S.; Figueroa, C. A.; Zanatta, A. R.; **Alvarez, F.***

In this work we report an experimental approach by combining in situ sequential top-down and bottom-up processes to induce the organization of nanosized nickel particles. The top-down process consists in xenon ion bombardment of a crystalline silicon substrate to generate a pattern, followed by depositing a similar to 15 nm titanium oxynitride thin film to act as a metallic diffusion barrier. Then, metallic nanoparticles are deposited by argon ion sputtering a pure nickel target, and the sample is annealed to promote the organization of the nickel nanoparticles (a bottom-up process). According to the experimental results, the surface pattern and the substrate biaxial surface strain are the driving forces behind the alignment and organization of the nickel nanoparticles. Moreover, the ratio between the F of metallic atoms arriving at the substrate relative to its surface diffusion mobility determines the nucleation regime of the nickel nanoparticles. These features are presented and discussed considering the existing technical literature on the subject.

AIP ADVANCES 8(1), 015025, 2018. DOI: 10.1063/1.499314

[P078-2018] "Statistical irreversible thermodynamics in the framework of zubarev's nonequilibrium statistical operator method"

Luzzi, R.*; Vasconcellos, A. R.*; Ramos, J. G.*; Rodrigues, C. G.

We describe the formalism of statistical irreversible thermodynamics constructed based on Zubarev's nonequilibrium statistical operator (NSO) method, which is a powerful and universal tool for investigating the most varied physical phenomena. We present brief overviews of the statistical ensemble formalism and statistical irreversible thermodynamics. The first can be constructed either based on a heuristic approach or in the framework of information theory in the Jeffreys-Jaynes scheme of scientific inference;

Zubarev and his school used both approaches in formulating the NSO method. We describe the main characteristics of statistical irreversible thermodynamics and discuss some particular considerations of several authors. We briefly describe how Rosenfeld, Bohr, and Prigogine proposed to derive a thermodynamic uncertainty principle.

THEORETICAL AND MATHEMATICAL PHYSICS 194(1), 4-29, 2018. DOI: 10.1134/S0040577918010038

[P079-2018] "Structural disorder effects on the magnetic entropy change of DyCo2 intermetallic: Mechanical milling and the weakening of the itinerant electron metamagnetism mechanism"

de Paula, V. G.*; Silva, M. G.; da Silva, L. M.; dos Santos, A. O.; Lang, R.; Otubo, L.; **Coelho, A. A.*; Cardoso, L. P.***

Magnetocaloric properties of the intermetallic DyCo2 compound (in the form of reduced size particles) and its correlations with the itinerant electron metamagnetism (IEM) phenomenon and structural disorders are investigated and discussed. Micrometric-sized particles were prepared by a mechanical milling technique for two low milling times (4 and 8 h) and characterized by means of X-ray diffraction, scanning and high-resolution transmission electron microscopy as well as magnetic measurements as a function of an applied external magnetic field and temperature. The results show that the particles have irregular-shaped and amorphous "edges/ledges" with embedded randomly oriented DyCo2 nanocrystallites. The average particle size practically does not change with increasing milling time, whereas the average crystallite size is slightly diminished. In contrast, microstrain values that indicate lattice deformation degree were rather increased after the milling processes. Structural disorders and surface effects, features resulting from mechanical impact, disturb the Dy-Co sublattice coupling and weaken the IEM mechanism responsible for the high magnetocaloric effect found for the DyCo2 bulk sample. For the milled samples, it was observed reductions in the peak intensity of the magnetic entropy change (-Delta S-M) and substantial broadenings of the distribution profiles which have contributed to an increase of the working temperature range of the investigated magnetocaloric material.

INTERMETALLICS 94, 1-9, 2018. DOI: 10.1016/j.intermet.2017.12.009

[P080-2018] "Structural transformations of carbon and boron nitride nanoscrolls at high impact collisions"

Woellner, C. F.*; Machado, L. D.; Autreto, P. A. S.; **de Sousa, J. M.*; Galvao, D. S.***

The behavior of nanostructures under high strain-rate conditions has been the object of theoretical and experimental investigations in recent years. For instance, it has been shown that carbon and boron nitride nanotubes can be unzipped into nanoribbons at high-velocity impacts. However, the response of many nanostructures to high strain-rate conditions is still unknown. In this work, we have investigated the mechanical behavior of carbon (CNS) and boron nitride nanoscrolls (BNS) colliding against solid targets at high velocities, using fully atomistic reactive (ReaxFF) molecular dynamics (MD) simulations. CNS (BNS) are graphene (boron nitride) membranes rolled up into papyrus-like structures. Their open-ended topology leads to unique properties not found in their close-ended analogs, such as nanotubes. Our results show that collision products are mainly determined by impact velocities and by two orientation angles, which define the position of the scroll (i) axis and (ii) open edge relative to the target. Our MD results showed that for appropriate velocities and orientations, large-scale deformations and nanoscroll fractures could occur. We also observed unscrolling (scrolls going back to quasi-planar membranes), scroll unzipping into nanoribbons, and significant reconstruction due to breaking and/or formation of new chemical bonds. For particular edge orientations and velocities, conversion from open to close-ended topology is also possible, due to the fusion of nanoscroll walls.

PHYSICAL CHEMISTRY CHEMICAL PHYSICS 20(7), 4911-4916, 2018. DOI: 10.1039/c7cp07402f

[P081-2018] "Studying the Ultraviolet Spectrum of the First Spectroscopically Confirmed Supernova at Redshift Two"

Smith, M.; Sullivan, M.; Nichol, R. C.; **Sobreira, F.***; et al.
DES Collaboration

We present observations of DES16C2nm, the first spectroscopically confirmed hydrogen-free superluminous supernova (SLSN-I) at redshift z approximate to 2. DES16C2nm was discovered by the Dark Energy Survey (DES) Supernova Program, with follow-up photometric data from the Hubble Space Telescope, Gemini, and the European Southern Observatory Very Large Telescope supplementing the DES data. Spectroscopic observations confirm DES16C2nm to be at z = 1.998, and spectroscopically similar to Gaia16apd (a SLSN-I at z = 0.102), with a peak absolute magnitude of U = -22.26 +/- 0.06. The high redshift of DES16C2nm provides a unique opportunity to study the ultraviolet (UV) properties of SLSNe-I. Combining DES16C2nm with 10 similar events from the literature, we show that there exists a homogeneous class of SLSNe-I in the UV (lambda(rest) approximate to 2500 angstrom), with peak luminosities in the (rest-frame) U band, and increasing absorption to shorter wavelengths. There is no evidence that the mean photometric and spectroscopic properties of SLSNe-I differ between low (z < 1) and high redshift (z > 1), but there is clear evidence of diversity in the spectrum at lambda(rest) < 2000 angstrom, possibly caused by the variations in temperature between events. No significant correlations are observed between spectral line velocities and photometric luminosity. Using these data, we estimate that SLSNe-I can be discovered to z = 3.8 by DES. While SLSNe-I are typically identified from their blue observed colors at low redshift (z < 1), we highlight that at z > 2 these events appear optically red, peaking in the observer-frame z-band. Such characteristics are critical to identify these objects with future facilities such as the Large Synoptic Survey Telescope, Euclid, and the Wide-field Infrared Survey Telescope, which should detect such SLSNe-I to z = 3.5, 3.7, and 6.6, respectively.

ASTROPHYSICAL JOURNAL 854(1), 37, 2018. DOI: 10.3847/1538-4357/aaa126

[P082-2018] "Systematic studies of correlations between different order flow harmonics in Pb-Pb collisions at root s(NN)=2.76 TeV"

Acharya, S.; Adam, J.; Adamova, D.; **Albuquerque, D. S. D.*; Chinellato, D. D.*; De Souza, R. D.*; Takahashi, J.***; et al.
ALICE Collaboration

The correlations between event-by-event fluctuations of anisotropic flow harmonic amplitudes have been measured in Pb-Pb collisions at root s(NN) = 2.76 TeV with the ALICE detector at the Large Hadron Collider. The results are reported in terms of multiparticle correlation observables dubbed symmetric cumulants. These observables are robust against biases originating from nonflow effects. The centrality dependence of correlations between the higher order harmonics (the quadrangular v(4) and pentagonal v(5) flow) and the lower order harmonics (the elliptic v(2) and triangular v(3) flow) is presented. The transverse momentum dependences of correlations between v(3) and v(2) and between v(4) and v(2) are also reported. The results are compared to calculations from viscous hydrodynamics and a multiphase transport (AMPT) model calculations.

The comparisons to viscous hydrodynamic models demonstrate that the different order harmonic correlations respond differently to the initial conditions and the temperature dependence of the ratio of shear viscosity to entropy density (eta/s). Asmall average value of eta/s is favored independent of the specific choice of initial conditions in the models. The calculations with the AMPT initial conditions yield results closest to the measurements. Correlations among the magnitudes of v(2), v(3), and v(4) show moderate p(T) dependence in midcentral collisions. This might be an indication of possible viscous corrections to the equilibrium distribution at hadronic freeze-out, which might help to understand the possible contribution of bulk viscosity in the hadronic phase of the system. Together with existing measurements of individual flow harmonics, the presented results provide further constraints on the initial conditions and the transport properties of the system produced in heavy-ion collisions.

PHYSICAL REVIEW C 97(2), 024906, 2018. DOI: 10.1103/PhysRevC.97.024906

[P083-2018] "The cosmological dark sector as a scalar sigma-meson field"

Carneiro, S.*

Previous quantum field estimations of the QCD vacuum in the expanding space-time lead to a dark energy component scaling linearly with the Hubble parameter, which gives the correct figure for the observed cosmological term. Here we show that this behaviour also appears at the classical level, as a result of the chiral symmetry breaking in a low energy, effective sigma--model. The dark sector is described in a unified way by the sigma condensate and its fluctuations, giving rise to a decaying dark energy and a homogeneous creation of non-relativistic dark particles. The creation rate and the future asymptotic de Sitter horizon are both determined by the sigma mass scale.

EUROPEAN PHYSICAL JOURNAL C 78(3), 183, 2018. DOI: 10.1140/epjc/s10052-018-5677-4

[P084-2018] "Time-Dependent Density Functional Theory Analysis of Triphenylamine-Functionalized Graphene Doped with Transition Metals for Photocatalytic Hydrogen Production"

Mota, E. A. V.; Neto, A. F. G.; **Marques, F. C.***; Mota, G. V. S.; Martins, M. G.; Costa, F. L. P.; Borges, R. S.; Neto, A. M. J. C.

The electronic structures and optical properties of triphenylamine-functionalized graphene (G-TPA) doped with transition metals, using water as a solvent, were theoretically investigated to verify the efficiency of photocatalytic hydrogen production with the use of transition metals. This study was performed by Density Functional Theory and Time-dependent Density Functional Theory through Gaussian 09W software, adopting the B3LYP functional for all structures. The 6-31g(d) basis set was used for H, C and N atoms, and the LANL2DZ basis set for transition metals using the Effective Core Potentials method. Two approaches were adopted: (1) using single metallic dopants (Ni, Pd, Fe, Os and Pt) and (2) using combinations of Ni with the other dopants (NiPd, NiPt, NiFe and NiOs). The DOS spectra reveal an increase of accessible states in the valence shell, in addition to a gap decrease for all dopants. This doping also increases the absorption in the visible region of solar radiation where sunlight is most intense (400 nm to 700 nm), with additional absorption peaks. The results lead us to propose the G-TPA structures doped with Ni, Pd, Pt, NiPt or NiPd to be novel catalysts for the conversion of solar energy for photocatalytic hydrogen production, since they improve the absorption of solar energy in the range of interest for solar radiation; and act as reaction centers, reducing the required overpotential for hydrogen production from water.

JOURNAL OF NANOSCIENCE AND NANOTECHNOLOGY 18[7], 4987-4991, 2018. DOI: 10.1166/jnn.2018.15277

[P085-2018] "Treatment of SU-8 surfaces using atmospheric pressure dielectric barrier discharge plasma"

Schianti, J. N.; do Nascimento, F.; Ramirez, J. C.; **Machida, M.***; Gabrielli, L. H.; Hernandez-Figueroa, H. E.; Moshkalev, S.

Dielectric barrier discharge (DBD) plasma was used to change the wettability of a SU-8 photoresist, reducing the contact angle and improving the surface smoothness. As most polymers, SU-8 has hydrophobic surfaces which prevents the adhesion of biological samples when used to fabricate biochemical sensors. Here, DBD Plasma treatment was conducted over the SU-8 surface, reducing the contact angle from 78 degrees to 12 degrees. The advantage of this treatment is that the SU-8 surface maintains the hydrophilic surface behavior over 24 h time period. DBD plasma modified the SU-8 surface wettability under low temperature variation and does not cause great irregularities on the surface. The highest value of root mean square surface roughness after 10min exposure was 2.9 +/- 0.3 nm. Published by the AVS.

JOURNAL OF VACUUM SCIENCE & TECHNOLOGY A 36(2), 021403, 2018. DOI: 10.1116/1.4999045

[P086-2018] "Ultralow and anisotropic thermal conductivity in semiconductor As2Se3"

Gonzalez-Romero, R. L.*; Antonelli, A.*; Chaves, A. S.*; Melendez, J. J.

An ultralow lattice thermal conductivity of 0.14 W m(-1) K-1 along the (b) over right arrow axis of As2Se3 single crystals was obtained at 300 K using first-principles calculations involving density functional theory and the resolution of the Boltzmann transport equation. This ultralow lattice thermal conductivity arises from the combination of two mechanisms: (1) a cascade-like fall of the low-lying optical modes, which results in avoided crossings of these with the acoustic modes, low sound velocities and increased scattering rates of the acoustic phonons; and (2) the repulsion between the lone-pair electrons of the As cations and the valence p orbitals of the Se anions, which leads to an increase in the anharmonicity of the bonds. The physical origins of these mechanisms lie in the nature of the chemical bonding in the material and its strong anisotropy. These results, whose validity has been addressed by comparison with SnSe, for which excellent agreement between the theoretical predictions and the experiments is achieved, point out that As2Se3 could exhibit improved thermoelectric properties.

PHYSICAL CHEMISTRY CHEMICAL PHYSICS 20(3), 1809-1816, 2018. DOI: 10.1039/c7cp07242b

[P087-2018] "Unusual effects of manual grinding and subsequent annealing process observed in Gd5.09Ge2.03Si1.88 compound"

Carvalho, A. M. G.; Alves, C. S.; Trevizoli, P. V.; dos Santos, A. O.; Gama, S.; **Coelho, A. A.***

The Gd5.09Ge2.03Si1.88 compound, as well as other magnetocaloric materials, certainly will not be used in their un-manufactured as-cast condition in future magnetic refrigeration applications or other devices. In this work, we have studied the Gd5.09Ge2.03Si1.88 compound processed in different ways, mainly, the as-cast powder, the annealed powder, and the pressed and sintered powder.

The annealed powder (1370 K/20 h) does not present the monoclinic phase and the first-order magneto-structural transition observed in the as-cast powder. The pressed and sintered powder also do not present the first-order transition. Furthermore, the compacting pressure shifts the second-order magnetic transition to lower temperatures. The behavior of cell parameters as a function of the compacting pressure indicates that T-C is directly affected by parameter c change.

APPLIED PHYSICS A-MATERIALS SCIENCE & PROCESSING 124(3), 269, 2018. DOI: 10.1007/s00339-018-1690-6

[P088-2018] "Voltage- and Light-Controlled Spin Properties of a Two-Dimensional Hole Gas in p-Type GaAs/AlAs Resonant Tunneling Diodes"

Galeti, H. V. A.; Gobato, Y. G.; **Brasil, M. J. S. P.***; Taylor, D.; Henini, M.

We have investigated the spin properties of a two-dimensional hole gas (2DHG) formed at the contact layer of a p-type GaAs/AlAs resonant tunneling diode (RTD). We have measured the polarized-resolved photoluminescence of the RTD as a function of bias voltage, laser intensity and external magnetic field up to 15T. By tuning the voltage and the laser intensity, we are able to change the spin-splitting from the 2DHG from almost 0 meV to 5 meV and its polarization degree from - 40% to + 50% at 15T. These results are attributed to changes of the local electric field applied to the two-dimensional gas which affects the valence band and the hole Rashba spin-orbit effect.

JOURNAL OF ELECTRONIC MATERIALS 47(3), 1780-1785, 2018. DOI: 10.1007/s11664-018-6065-4

[P089-2018] "Evidence of ghost suppression in gluon mass scale dynamics"

Aguilar, A. C.*; Binosi, D.; **Figueiredo, C. T.***; Papavassiliou, J.

In this work we study the impact that the ghost sector of pure Yang-Mills theories may have on the generation of a dynamical gauge boson mass scale, which hinges on the appearance of massless poles in the fundamental vertices of the theory, and the subsequent realization of the well-known Schwinger mechanism. The process responsible for the formation of such structures is itself dynamical in nature, and is governed by a set of Bethe-Salpeter type of integral equations. While in previous studies the presence of massless poles was assumed to be exclusively associated with the background-gauge three-gluon vertex, in the present analysis we allow them to appear also in the corresponding ghost-gluon vertex. The full analysis of the resulting Bethe-Salpeter system reveals that the contribution of the poles associated with the ghost-gluon vertex are particularly suppressed, their sole discernible effect being a slight modification in the running of the gluon mass scale, for momenta larger than a few GeV. In addition, we examine the behavior of the (background-gauge) ghost-gluon vertex in the limit of vanishing ghost momentum, and derive the corresponding version of Taylor's theorem. These considerations, together with a suitable Ansatz, permit us the full reconstruction of the pole sector of the two vertices involved.

EUROPEAN PHYSICAL JOURNAL C 78(3), 181, 2018. DOI: 10.1140/epjc/s10052-018-5679-2

Eventos publicados

[P090-2018] "Diffusive-like effects and possible non trivial local topology on the half-Heusler YPdBi compound"

Souza, J. C.*; Lesseux, G. G.*; Urbano, R. R.*; Rettori, C.*; Pagliuso, P. G.*

The non-ambiguous experimental identification of topological states of matter is one of the main interesting problems regarding this new quantum state of matter. In particular, the half-Heusler family RMT (R = rare-earth, T = Pd, Pt or Au and T = Bi, Sb, Pb or Sn) could be a useful platform to explore these states due to their cubic symmetry and the topological properties tunable via their unit cell volume and/or the nuclear charges of the M and T atoms. In this work, we report electron spin resonance (ESR) and complementary macroscopic measurements in the Nd-3 (+) -doped putative topologically trivial semimetal YPdBi. Following the Nd-3 (+) ESR lineshape as a function of microwave power, size of the particle and temperature, we have been able to observe an evolution from a Dysonian lineshape to a diffusive-like lineshape. Furthermore, the Nd-3 (+) ESR intensity saturation is concentration dependent, which could be due to a phonon-bottleneck process. Comparing these results with the Nd-3 (+) -doped YPtBi, we discuss a possible scenario in which the Nd-3 (+) ions could locally tune the topological properties of the system.

AIP ADVANCES 8(5), 055713, 2018. DOI: 10.1063/1.5007623

62nd Annual Conference on Magnetism and Magnetic Materials (MMM), NOV 06-10, 2017, Pittsburgh, PA.

[P091-2018] "Magnetic upconverting fluorescent NaGdF4:Ln(3+) and iron-oxide@NaGdF4:Ln(3+) nanoparticles"

Shrivastava, N.; Rocha, U.; **Muraca, D.*;** Jacinto, C.; Moreno, S.; Vargas, J. M.; Sharma, S. K.

Microwave assisted solvothermal method has been employed to synthesize multifunctional upconverting beta--NaGdF4:Ln(3+) and magnetic-upconverting Fe3O4/gamma Fe2O3@NaGdF4:Ln(3+) (Ln = Yb and Er) nanoparticles. The powder x-ray diffraction data confirms the hexagonal structure of NaGdF4:Ln(3+) and high resolution transmission electron microscopy shows the formation of rod shaped NaGdF4:Ln3(+) (similar to 20 nm) and ovoid shaped Fe3O4/gamma-Fe2O3@ NaGdF4:Ln(3+) (similar to 15 nm) nanoparticles. The magnetic hysteresis at 300 K for beta-NaGdF4:Ln(3+) demonstrates paramagnetic features, whereas iron-oxide@beta-NaGdF4:Ln(3+) exhibits superparamagnetic behavior along with a linear component at large applied field due to paramagnetic NaGdF4 matrix. Both nanoparticle samples provide an excellent green emitting [(H-2(11/2), S-4(3/2))-> I-4(15/2) (similar to 540 nm)] upconversion luminescence emission under excitation at 980 nm. The energy migration between Yb and Er in NaGdF4 matrix has been explored from 300-800 nm. Intensity variation of blue, green and red lines and the observed luminescence quenching due to the presence of Fe3O4/gamma-Fe2O3 in the composite has been proposed. These kinds of materials contain magnetic and luminescence characteristics into single nanoparticle open new possibility for bioimaging applications.

AIP ADVANCES 8(5), 056710, 2018. DOI: 10.1063/1.5007748

62nd Annual Conference on Magnetism and Magnetic Materials (MMM), NOV 06-10, 2017, Pittsburgh, PA.

Correções

[Co001-2018] "Combined fit of spectrum and composition data as measured by the Pierre Auger Observatory (vol 4, 038, 2017)"

Aab, A.; Abreu, P.; Aglietta, M.; **Chinellato, J. A.*; Daniel, B.*; Diaz Castro, M. L.*; Dobrigkeit, C.*; Fauth, A. C.*; Kemp, E.*;**

Muller, M. A.*; Pereira, L. A. S.*; Theodoro, V. M.*; et al.
Pierre Auger Collaboration

JOURNAL OF COSMOLOGY AND ASTROPARTICLE PHYSICS 3, E02, 2018. DOI: 10.1088/1475-7516/2018/03/E02

[Co002-2018] "Search for dark matter and unparticles in events with a Z boson and missing transverse momentum in proton-proton collisions at root s = 13 TeV (vol 9, 106, 2017)"

Sirunyan, A. M.; Tumasyan, A.; Adam, W.; **Chinellato, J. A.*; Tonelli Manganote, E. J.***; et al.
CMS Collaboration

JOURNAL OF HIGH ENERGY PHYSICS 1, 056, 2018. DOI: 10.1007/JHEP01(2018)056

***Autores da comunidade IFGW**
Fonte: Web of Science on-line.

Defesas de Dissertações do IFGW

[D002-2018] "Um modelo cosmológico inspirado em um plasma de quark-gluons"
Aluno: Melissa Mendes Silva
Orientador: Prof. Dr. Donato Giorgio Torrieri
Data: 27/02/2018

[D003-2018] "Estudo e Caracterização via Simulação Monte Carlo de Danos de Radiação Ionizante em Detectores de Pixel Híbrido"
Aluno: Débora de Paiva Magalhães
Orientador: Profa. Dra. Alessandra Tomal
Data: 23/03/2018

[D004-2018] "Máquinas de Szilárd Microcanônicas e Quebras Espontâneas de Simetria"
Aluno: Artur Soriani Alves
Orientador: Prof. Dr. Marcus Vinicius Segantini Bonança
Data: 12/04/2018

[D005-2018] "Otimização dos parâmetros de exposição em mamografia digital: estudos experimentais e por simulação Monte Carlo"
Aluno: Rodrigo Trevisan Massera
Orientador: Profa. Dra. Alessandra Tomal
Data: 12/04/2018

[D006-2018] "Engenharia de dispersão e geração de pentes de frequência em microdiscos de óxido de silício"
Aluno: Laís Fujii dos Santos
Orientador: Prof. Dr. Gustavo Silva Wiederhecker
Data: 27/04/2018

[D007-2018] "Estudo da Anisotropia Dipolar de Raios Cósmicos Detectados no Observatório Pierre Auger e de sua Dependência da Declinação"
Aluno: Danelise de Oliveira Franco
Orientador: Profa. Dra. Carola Dobrigkeit Chinellato
Data: 28/05/2018

Defesas de Teses do IFGW

[T006-2018] "Transporte Eletrônico em Conjuntos Moleculares Semicondutores"
Aluno: Leandro das Mercês Silva
Orientador: Prof. Dr. Carlos César Bof Bufon
Data: 19/03/2018

[T007-2018] "Investigação das propriedades óptico-estruturais de filmes finos de TiO2 dopados com íons terras-raras para o desenvolvimento de novos materiais emissores de luz"
Aluno: Diego L. Silva Scoca
Orientador: Prof. Dr. Fernando Alvarez
Data: 23/03/2018

[T008-2018] "O Uso de Medidas Fracas Ópticas no Estudo de Fenômenos Associados a Desvios de Feixes Gaussianos"
Aluno: Gabriel Gulak Maia
Orientador: Prof. Dr. Stefano de Leo
Data: 28/03/2018

[T009-2018] "Optical Image Cloning"
Aluno: Shamaila Manzoor
Orientador: Prof. Dr. Luís Eduardo Evangelista de Araújo
Data: 04/04/2018

[T010-2018] "Modificação de Hábito e Análise Estrutural de Monocristais Quase Perfeitos de NaBrO3 Dopados com S2O6 por Difração de Raios X de n-Feixes e Absorção"
Aluno: Guilherme Calligaris de Andrade
Orientador: Prof. Dr. Lisandro Pavie Cardoso
Data: 25/04/2018

Fonte: Portal IFGW/Pós-graduação - Agenda de Colóquios, Defesas e Seminários.
Disponível em: http://portal.ifi.unicamp.br/pos-graduacao

Abstracta

Instituto de Física
Diretor: Prof. Dr. Pascoal José Giglio Pagliuso
Diretora Associada: Profa. Dra. Mônica Alonso Cotta
Universidade Estadual de Campinas - UNICAMP
Cidade Universitária Zeferino Vaz
13083-859 - Campinas - SP - Brasil
e-mail: secdir@ifi.unicamp.br
Fone: +55 19 3521-5300

Publicação

Biblioteca do Instituto de Física Gleb Wataghin
http://portal.ifi.unicamp.br/biblioteca

Diretora Técnica: Sandra Maria Carlos Cartaxo
Coordenadora da Comissão de Biblioteca: Profa. Dra. Arlene Cristina Aguilar

Elaboração:
Maria Graciele Trevisan (Bibliotecária)
Ayres Neri da Cunha Junior
contato: infobif@ifi.unicamp.br